To Appear in *The Astrophysical Journal*

X-RAYS FROM NGC 3256: HIGH-ENERGY EMISSION IN STARBURST GALAXIES AND THEIR CONTRIBUTION TO THE COSMIC X-RAY BACKGROUND

EDWARD C. MORAN[1,2]

Department of Astronomy, University of California
Berkeley, CA 94720-3411

MATTHEW D. LEHNERT[2,3]

Leiden Observatory
Postbus 9513, 2300RA, Leiden, The Netherlands

AND

DAVID J. HELFAND[4]

Department of Astronomy, Columbia University
New York, NY 10027

ABSTRACT

The infrared-luminous galaxy NGC 3256 is a classic example of a merger-induced nuclear starburst system. We find here that it is the most X-ray–luminous star-forming galaxy yet detected ($L_{0.5-10\,\mathrm{keV}} = 1.6 \times 10^{42}\,\mathrm{ergs\,s^{-1}}$). Long-slit optical spectroscopy and a deep, high-resolution *ROSAT* X-ray image show that the starburst is driving a "superwind" which accounts for $\sim 20\%$ of the observed soft X-ray emission. Analysis of X-ray spectral data from *ASCA* indicates this gas has a characteristic temperature of $kT \approx 0.3$ keV. Our model for the broadband X-ray emission of NGC 3256 contains two additional components: a warm thermal plasma ($kT \approx 0.8$ keV) associated with the central starburst, and a hard power-law component with an energy index of $\alpha_{\mathrm{X}} \approx 0.7$. We discuss the energy budget for the two thermal plasmas and find that the input of mechanical energy from the starburst is more than sufficient to sustain the observed level of emission. We also examine possible origins for the power-law component, concluding that neither a buried AGN nor the expected population of high-mass X-ray binaries can account for this emission. Inverse-Compton scattering, involving the galaxy's copious flux of infrared photons and the relativistic electrons produced by supernovae, is likely to make a substantial contribution to the hard X-ray flux. Such a model is consistent with the observed radio and IR fluxes and the radio and X-ray spectral indices. We explore the role of X-ray–luminous starbursts in the production of the cosmic X-ray background radiation. The number counts and spectral index distribution of the faint radio source population, thought to be dominated by star-forming galaxies, suggest that a significant fraction of the hard X-ray background could arise from starbursts at moderate redshift.

Subject headings: diffuse radiation — galaxies: individual (NGC 3256) — galaxies: starburst — X-rays: galaxies

---

[1] Chandra Fellow.

[2] Participating Guest, Institute of Geophysics and Planetary Physics, Lawrence Livermore National Laboratory, Livermore, CA.

[3] Visiting observer at Cerro Tololo Inter-American Observatory of the National Optical Astronomy Observatories, operated by Aura, Inc. under contract with the National Science Foundation.

[4] Also Institute of Astronomy, University of Cambridge, Cambridge, UK.

1. Introduction

The spectacular nearby[5] southern galaxy NGC 3256, with a highly disturbed central region and bright, extended tidal tails, is an excellent example of a merging system. Based on its extreme brightness in the near infrared and strong narrow optical emission-line spectrum, NGC 3256 is considered to be a "super starburst" galaxy (Joseph & Wright 1985), in the midst of an especially vigorous episode of star formation. The starburst and merger events are expected, ultimately, to render NGC 3256 a gas-depleted elliptical galaxy (Graham et al. 1984).

NGC 3256 is seemingly a luminous X-ray source as well. It was one of 20 "normal" galaxies from the *ROSAT* All-Sky Survey (RASS) reported to have Seyfert-like X-ray luminosities (Boller et al. 1992). While most of these X-ray sources did, in fact, prove to be previously unrecognized active galaxies (Moran, Halpern, & Helfand 1994), the identification of NGC 3256 as an X-ray source and its classification as a starburst galaxy remain secure. The soft (0.1–2.4 keV) X-ray luminosity of NGC 3256, originally listed as $L_{\rm X} = 2 \times 10^{42}\,{\rm ergs\,s^{-1}}$ (Boller et al. 1992), would distinguish it as the most luminous X-ray starburst galaxy currently known (see Fabbiano 1989).

X-ray observations offer valuable insight into the starburst phenomenon and the cosmological significance of starburst galaxies. For example, soft X-ray images have revealed ionized gas in the halos of several starburst galaxies (e.g., Fabbiano 1988), which long-slit optical spectroscopy has indicated is being driven outward from their nuclear regions (e.g., McCarthy, Heckman, & van Breugel 1987; Lehnert & Heckman 1996). The ultimate fate of this gas has direct consequences for a number of important outstanding astrophysical problems, such as the evolution of galaxies and the heating and enrichment of the intergalactic medium (Heckman 1998). X-ray–luminous starburst galaxies may also represent a significant component of the cosmic X-ray background (XRB; Bookbinder et al. 1980; Stewart et al. 1982; Griffiths & Padovani 1990), although to do so, they would have to exhibit very flat spectra in the hard X-ray band in order to explain the shape of the XRB spectrum (Fabian & Barcons 1992).

NGC 3256, because of its apparently exceptional X-ray luminosity, offers a unique opportunity to investigate these issues. Furthermore, with an infrared luminosity of $\sim 6 \times 10^{11}\ L_{\odot}$ (Sargent, Sanders, & Phillips 1989), NGC 3256 is nearly an "ultraluminous" infrared galaxy. Hard X-ray observations of this object could also be used to search for a buried active nucleus and, thus, to comment on the proposition that ultraluminous infrared galaxies are linked to the origin of quasars (Sanders et al. 1988). In this paper, we explore both the soft and hard X-ray properties of NGC 3256 using observations obtained with the *ROSAT* and *ASCA* satellites. In combination with spatially resolved optical spectroscopy and the results of published radio and infrared studies, these data shed new light on the nature of the prodigious burst of star formation in NGC 3256.

In § 2, we present optical evidence for a galactic "superwind" driven by the starburst activity in NCG 3256. We then present the X-ray imaging and spectroscopic data we have collected on this galaxy (§ 3). We interpret the X-ray emission as arising from three distinct components (§ 4): thermal emission from both the superwind and supernova-heated gas in the galactic disk, and a nonthermal component, which is likely to arise from X-ray binary star systems and inverse-Compton scattered radiation in the nuclear region of the galaxy. We close with a discussion of the implications of our analysis for the origin of the cosmic X-ray background.

2. Optical Spectroscopy of NGC 3256

Optical spectroscopy provides valuable information regarding the properties of the ionized gas in galaxies, such as its location, velocity, density, pressure, ionization state, and heavy-element

[5] $D = 56$ Mpc for $z = 0.0094$ and a Hubble constant of $H_0 = 50$ km s^{-1} Mpc^{-1}, which we use throughout this paper.

abundances. Long-slit spectra of NGC 3256 were acquired on the night of 1993 March 22 (UT) with the CTIO 4 m telescope in combination with the R-C Spectrograph. The spectra, which have a resolution of 5.6 Å (FWHM) and cover a wavelength range of 4760–6800 Å, were obtained using a 2.″5 slit oriented at position angles (PAs) of 65° and 155° (east of north). The exposure times for the spectra were 900 s (PA = 65°) and 1200 s (PA = 155°). Flux calibration was performed using exposures of the stars L745-46A, LTT 2415, and LTT 7379 taken at the beginning and end of the night through a 10″ slit. The spectra were summed into 3-column (2.″4) bins in the spatial direction prior to extraction. For each extracted spectrum, we measured the fluxes and velocity widths of the following emission lines: Hβ, [O III] λ5007, [N I] λ5199, [O I] λ6300, Hα, [N II] λ6583, and [S II] $\lambda\lambda$6716,6731. We corrected the fluxes of Hα and Hβ for absorption due to the underlying stellar continuum by assuming this absorption has an equivalent width of 5 Å at both wavelengths;[6] the resultant Hα/Hβ ratios were then used to estimate the reddening of each spectrum, under the assumption that Hα/Hβ has an intrinsic value of 2.86 (appropriate for Case B recombination and a gas temperature of 10^4 K; Osterbrock 1989). Based on these reddening estimates, we corrected the measured emission-line fluxes using the standard extinction curve from Osterbrock (1989).

2.1. *Emission-Line Evidence for a Starburst-Driven "Superwind"*

Observations of nearby edge-on starburst galaxies have revealed both extended optical emission-line regions and plumes of soft X-ray emission along the minor axes of these objects, indicating the presence of ionized gas in their halos (e.g., McCarthy et al. 1987; Fabbiano 1988; Heckman, Armus, & Miley 1990; Armus et al. 1995; Lehnert & Heckman 1995, 1996). The optical emission lines from the extraplanar gas exhibit (1) signatures of a complex velocity field (i.e., multiple velocity components, velocity shear, and velocity widths that increase with increasing distance from the nucleus), and (2) "shock-like" flux ratios (i.e., enhancements of the low-ionization [O I], [O II], [N II], and [S II] lines relative to Hα) similar to those that characterize low-ionization nuclear emission-line regions (LINERs; Heckman 1980). Together, these properties suggest that the heating and kinematics of the ionized halo gas are coupled through shocks, consistent with the interpretation that this gas arises from a galactic-scale outflow driven by supernovae in the starburst nucleus (a "superwind"; Heckman et al. 1990). The approximately face-on orientation of NGC 3256 ($i \approx 30°$–$40°$; Feast & Robertson 1978; Moorwood & Oliva 1994) makes it difficult to locate the extended line-emitting regions along the line of sight, and, thus, to compare its emission-line properties directly with those of edge-on starburst galaxies. However, if NGC 3256 does possess a superwind, we might expect it to display the signatures of a wind far from the nucleus, where the emission is less dominated by the intense UV field of the bright nuclear H II regions (see Lehnert & Heckman 1996).

Reddening- and absorption-corrected emission-line flux ratios for NGC 3256 are plotted in Figures 1 and 2 as a function of projected distance from the nucleus along PA = 65°and PA = 155°, respectively. Line emission is detected up to half an arcminute (8 kpc) away from the nucleus. Within the central 10″, the line flux ratios are consistent with those of H II regions (Veilleux & Osterbrock 1987): log [O III]/H$\beta \approx -0.7$, log [N II]/H$\alpha < -0.3$, log [O I]/H$\alpha \approx -1.7$, and log [S II]/H$\alpha \approx -0.8$. Outside the nuclear region, however, these line ratios increase dramatically, becoming more "LINER-like" with increasing distance from the nucleus: log [N II]/H$\alpha \approx -0.2$, log [O I]/H$\alpha > -1.0$, and log [S II]/H$\alpha > -0.3$. Figure 3 illustrates the differences between the nuclear and off-nuclear spectra of NGC 3256 (the off-nuclear spectra are discussed further in the

[6] The value of 5 Å for the equivalent width of the stellar absorption features at Hα and Hβ was estimated using high-resolution ($\sim$ 1 Å) spectra of NGC 3256 taken in the Hβ region along PA = 155°. Where the S/N ratio was sufficient (i.e., within $\sim$ 10″ of the nucleus), the wings of the Hβ absorption line were clearly resolved in these data. Fitting the wings yielded absorption-line strengths of 5$\pm$1 Å. This is likely to be the largest correction necessary; thus, the off-nuclear line ratios we derive are, if anything, underestimated.

next section). The velocity widths of the strongest emission lines also increase with increasing distance from the nucleus, as indicated in Figure 4. In fact, a comparison of Figures 2 and 4 reveals that LINER-like emission-line flux ratios are produced in the *same* regions where the line velocity widths are greatest. This correspondence is demonstrated more clearly in Figure 5, which shows that the [O I]/Hα flux ratio is correlated with the width of the Hα line.

The coupling between the emission-line flux ratios and velocity widths in NGC 3256 suggests that the ionization and kinematics of the extranuclear emission-line gas are strongly influenced by shocks. Thus, in most respects, the extended ionized gas in NGC 3256 displays the same characteristics as the wind-driven halo gas observed in edge-on starburst galaxies (cf. Lehnert & Heckman 1996). We note that, because of the roughly face-on orientation of NGC 3256, we cannot rule out the possibility that some of the extended line emission is contributed by a diffuse ionized medium (DIM) within the galaxy. The DIM observed in the Milky Way (Reynolds 1990; Lehnert & Heckman 1994) and the disks of late-type spiral galaxies (Wang, Heckman, & Lehnert 1997) also exhibits strong low-ionization emission lines relative to Hα. However, the velocity widths, flux ratios, and surface brightness of the emission lines associated with the DIM in other galaxies (Wang et al. 1997) are much less extreme than the quantities observed for the gas in the off-nuclear regions of NGC 3256. Thus, it is unlikely that a DIM in NGC 3256, if present, dominates the extended line emission. We conclude, therefore, that the starburst in NGC 3256 must be driving a superwind. As we discuss in § 3.1, this conclusion is entirely consistent with the galaxy's soft X-ray morphology.

2.2. *Broad Off-Nuclear Hα Emission*

As illustrated in Figure 3, there appears to be a prominent broad Hα emission line in the off-nuclear spectra of NGC 3256. Surprisingly, the broad line is present on either side of the nucleus in both sets of spectra we obtained. The onset of this feature in our $2\farcs4 \times 2\farcs5$ extractions occurs between $7''$ and $15''$ from the nucleus. In these spectra, the broad Hα wings have a full-width at zero-intensity (FWZI) of $\sim (4-6) \times 10^3$ km s^{-1}. The line has a FWZI of $\sim 6 \times 10^3$ km s^{-1} in the larger $8'' \times 2\farcs5$ extractions displayed in Figure 3, and does not appear to be shifted significantly relative to the narrow component of Hα.

Because of the broad Hα line, the off-nuclear spectra bear a remarkable resemblance to the spectra of active galactic nuclei. However, since this emission is detected in *all* of the extended emission-line regions we examined, the possibility that we are observing AGN light directly is immediately ruled out. A scenario in which NGC 3256 contains an obscured AGN whose broad Hα emission is scattered in our direction by an off-nuclear "mirror" is equally implausible: the combined effects of (1) the large distance between the nucleus and the scattering medium, (2) the considerable extinction the AGN light would be likely to suffer en route to this medium, and (3) the low expected scattering efficiency, suggest that a buried AGN, if present, would have to be intrinsically very luminous. Although such an object could be hidden from our optical view, it would be readily detectable in the radio, mid-infrared, and hard X-ray bands; as we discuss in § 4.3.1, there is no evidence at any of these wavelengths for a luminous, obscured AGN in NGC 3256.

The broad off-nuclear Hα line must, therefore, be related to the star-formation or merger activity in NGC 3256. Unfortunately, examples of starburst galaxies with similar features are scarce. For instance, in the extensive survey of edge-on starburst galaxies conducted by Lehnert & Heckman (1995), none of the ~ 50 galaxies presented exhibits this characteristic. Although weak, broad Hα emission with FWZI $\approx$ 2000–3000 km s^{-1} has been observed in a few star-forming galaxies, the broad lines have been attributed to highly localized phenomena, such as compact super-star clusters (e.g., Heckman et al. 1995) or knots of Wolf-Rayet stars (e.g., Sargent & Filippenko 1991). Once again, neither of these explanations seems viable for NGC 3256 since the broad Hα line is observed throughout the extranuclear emission-line regions. For this reason, we suspect that the extended broad Hα emission in NGC 3256 is somehow associated with the galaxy's starburst-driven wind (cf. Tenorio-Tagle et al. 1997). It is possible that the roughly face-on orientation of

NGC 3256 has made the detection of this intrinsically faint feature easier than it would be if the system were edge-on. Alternatively, the line may be enhanced in this object because of the ongoing merger activity, which is likely to have disturbed the gas in the galaxy considerably (e.g., Mihos & Hernquist 1996). Comparable data on the extended emission-line properties of other face-on, merging starburst galaxies is very limited, making it difficult to assess the relative importance of these factors.

2.3. *Chemical Abundance of the Nuclear Emission-Line Gas*

We have applied the empirical method of Edmunds & Pagel (1984) to constrain the heavy-element abundances of the nuclear emission-line gas, which will assist our modelling of the X-ray spectrum in § 3.2. This method employs reddening-corrected [O III]/Hβ and [O III]/[N II] ratios and assumes that the excitation processes in the nuclear region of NGC 3256 are similar to those in the H II regions of nearby galaxies. As discussed above, this appears to be the case. From our dereddened nuclear spectra of NGC 3256, we find log [O III]/Hβ = -0.53 and log [O III]/[N II] = -0.92. These ratios imply an oxygen abundance of 9.1 ± 0.2 (on the scale 12 + log [O/H]), which is approximately 0.2 dex above the solar value. The uncertainty in this estimate includes only the uncertainty in the calibration of Edmunds & Pagel (1984) and does not reflect possible errors in our measurements of the line ratios. The latter, however, are relatively small, and we conclude that metal abundances in the ionized gas in the nucleus of NGC 3256 are approximately solar. In § 4.2.3 we present analysis which suggests that the abundances of the extended ionized gas in NGC 3256 are similar to those in the nuclear region.

3. X-Ray Observations of NGC 3256

NGC 3256 was the target of a 3.4 ks pointed observation with the *ROSAT* Position Sensitive Proportional Counter (PSPC) on 1992 January 14. We acquired these data from the HEASARC archive at NASA Goddard Space Flight Center. Source counts were collected within a circular region $1'$ in radius. Subtraction of the background, which was measured in an annulus with inner and outer radii of $3'$ and $9'$ centered on the galaxy, resulted in the detection of 227 source counts in the 0.1–2.4 keV band. We rebinned the PSPC spectrum so that it had at least 20 counts per energy channel.

The X-ray source in NGC 3256 appears to be marginally resolved in the PSPC image, which has an angular resolution of $\sim 30''$. To obtain a more accurate determination of the spatial extent of the X-ray emission, we observed the galaxy with the High Resolution Imager (HRI) on board *ROSAT* for 54.0 ks on 1995 December 10. The HRI provides $\sim 5''$ resolution, also in the 0.1–2.4 keV band. A total of 1412 counts above the background were detected within a $1'$ radius region centered on the galaxy.

We also observed NGC 3256 in the 0.5–10 keV range with the *ASCA* satellite (Tanaka, Inoue, & Holt 1994) on 1993 December 6. Total exposures of 33.2 and 32.4 ks were obtained with *ASCA*'s Solid-state Imaging Spectrometers SIS0 and SIS1, respectively, which were operated in 1-CCD mode. An exposure of 36.1 ks was achieved with each of the two Gas Imaging Spectrometers (GIS2 and GIS3) on board *ASCA*. Periods of high background were filtered from the photon event files for each instrument following the guidelines described in The ABC Guide to *ASCA* Data Reduction (Day et al. 1995). Source counts were collected within circular regions $3'$ (SIS) and $6'$ (GIS) in radius centered on the galaxy. The SIS background was measured in source-free areas on the chip. In the GIS images, background was measured in a region with twice the area of the source region located approximately the same distance off-axis as NGC 3256. The background-subtracted spectra obtained with the SIS0, SIS1, GIS2, and GIS3 instruments contain 1116, 1039, 786, and 1000 counts, respectively. For spectral modeling (§ 3.2), we combined the two SIS spectra and the

two GIS spectra using the FTOOLS task "addascaspec." The resultant spectra were rebinned to have a minimum of 40 (SIS) or 80 (GIS) counts (source plus background) per energy channel.

3.1. *Extended Soft X-Ray Emission*

An important key to the nature of the X-ray emission from NGC 3256 is its spatial extent. With an angular resolution of $\sim 5''$, the *ROSAT* HRI is best suited to provide this information. Unfortunately, NGC 3256 is sufficiently distant that features in the galaxy smaller than ~ 1 kpc in size are unresolved with the HRI. But as the HRI image displayed in Figure 6 indicates, the soft X-ray flux from NGC 3256 is significantly more extended than this. Although confined to the main body of the galaxy, the soft X-ray emission spans $45''$ in diameter, or ~ 12 kpc. The X-ray flux peaks near the optical nucleus at $\alpha(2000) = 10^{\rm h}27^{\rm m}51\overset{\rm s}{.}4$, $\delta(2000) = -43^\circ 54' 15''$, but a dominant central source, which we would expect if an active nucleus were responsible for most of the emission, is not present. In the full-resolution HRI image ($1''$ pixels, unsmoothed), just 110 counts fall within a $5'' \times 5''$ detection cell centered on the X-ray peak; as half the power of the on-axis HRI point-response function is contained in a cell of this size (David et al. 1997), we derive a firm upper limit of 16% for the contribution of a nuclear point source to the HRI counts. The soft X-ray half-light radius is about $11''$.

Soft X-ray emission extended over several kiloparsecs is a common property of starburst galaxies driving hot, outflowing winds, such as in the prototypical starburst M82 (Moran & Lehnert 1997, and references therein; see also Strickland, Ponman, & Stevens 1997), NGC 253 (Fabbiano 1988), NGC 1569 (Heckman et al. 1995), NGC 1808 (Dahlem, Hartner, & Junkes 1994), NGC 2146 (Armus et al. 1995), NGC 3628 (Dahlem et al. 1996), NGC 4449 (Della Ceca, Griffiths, & Heckman 1997), and Arp 220 (Heckman et al. 1996). As discussed in § 2.1, there is ample optical evidence that the starburst in NGC 3256 is also driving a wind, and much of the extended HRI flux we observe is likely to be associated with this hot gas. The X-ray spectrum of NGC 3256, presented in the next section, provides further details regarding the origin and nature of this emission.

3.2. *Broadband X-Ray Spectroscopy*

A comprehensive understanding of the X-ray properties of NGC 3256 is only possible through the analysis of its emission over a wide bandpass, which our *ASCA* observation in the 0.5–10 keV range provides. Although *ROSAT* is sensitive down to 0.1 keV, very few counts were detected below 0.5 keV in the short PSPC exposure because of the sizable Galactic column density in the direction of NGC 3256 ($N_{\rm H} = 9.6 \times 10^{20}$ cm^{-2}). The low S/N ratio PSPC data do not augment the *ASCA* spectra and are, therefore, omitted from our broadband analysis, although the measured count rates for both the PSPC and HRI detections are consistent with the model we derive.

We fitted the SIS and GIS spectra of NGC 3256 simultaneously, employing a variety of models; the results are summarized in Table 1. The extended nature of the soft X-ray emission and the optical evidence for a starburst-driven wind makes a Raymond-Smith (R-S) plasma an obvious model with which to fit these spectra. Furthermore, as we demonstrate below, strong emission lines are plainly visible in the *ASCA* spectra, confirming the presence of a hot, optically thin gas. But a single R-S component with solar heavy-element abundances (§ 2.3; see also §4.2.3) provides a very poor fit to the data ($\chi^2 = 207$ for 82 degrees of freedom), so we must consider more complex models.

As Table 1 indicates, two-component models involving a "warm" R-S plasma and a harder R-S or power law (PL; $F_E \propto E^{-\Gamma}$) component provide much better fits to the *ASCA* spectra of NGC 3256. In particular, the fits in which the absorption column densities applied to the two components are independent yield values of χ^2_ν ($= \chi^2/\nu$, where ν is the number of degrees of freedom) of roughly unity. In these models, the characteristic temperature of the warm component is $kT \approx 0.7$ keV; the hard component has a characteristic temperature of $kT \approx 12$ keV or a

photon index $\Gamma \approx 1.7$. The *ASCA* spectra of NGC 3256, fitted with the (PL + R-S) model,[7] are displayed in Figure 7*a*. Note that the hard component dominates the X-ray flux below 0.7 keV as well as above $\sim$ 1.5 keV. A nearly identical circumstance was encountered when a (PL + R-S) model was applied to the broadband X-ray spectrum of the starburst galaxy NGC 4449 (Della Ceca et al. 1997). However, the dissimilarity of the very soft and hard X-ray morphologies of that galaxy, which should be the same if a single component dominates in each band, provided sufficient grounds for the rejection of two-component models for that object. In the case of NGC 3256, the specific absorption scenario suggested in the best two-component models also calls such models into question. Despite the significant Galactic column density toward NGC 3256 ($\sim 10^{21}$ cm^{-2}), the best-fit absorption column for the hard component is zero, whereas the absorption derived for the warm R-S component is seven to eight times *higher* than the Galactic value. Although the formal 90% confidence ranges for both column densities are large (see Table 1), they do not overlap, implying that, in these models, the warm R-S component must be more absorbed. This is the reverse of the situation found for other starburst galaxies with sufficiently high S/N ratio broadband X-ray spectra (e.g., Awaki et al. 1996; Moran & Lehnert 1997): the softest thermal emission is more spatially extended and less absorbed than the hard X-ray component. For the absorption of the hard X-ray source in NGC 3256 to be comparable to or greater than that of the warm thermal component would require the existence of an additional source of soft X-ray emission in the galaxy.

Unfortunately, the statistical quality of the *ASCA* spectra of NGC 3256 is barely adequate for the application of more detailed models. Nonetheless, it is becoming clear that the broadband X-ray spectra of starburst galaxies are, in fact, quite complex. For example, in our *ROSAT* and *ASCA* study of the nearby starburst M82 (Moran & Lehnert 1997), we showed that at least three spectral components are required to fit its high S/N ratio 0.1–10 keV spectrum. The M82 model consisted of a hard $\Gamma = 1.7$ power law, a warm $kT = 0.6$ keV R-S component, and a soft $kT = 0.3$ keV R-S component. We found that while the hard and warm components are heavily absorbed ($N_{\rm H} \approx 10^{22}$ cm^{-2}), the soft R-S component is not absorbed above the Galactic column. A nearly identical model was determined for the *ASCA* spectrum of the starburst galaxy NGC 1808 by Awaki et al. (1996). Similarly, a three-component model was favored in the analysis of the broadband X-ray spectrum of NGC 4449 (Della Ceca et al. 1997).

Motivated by these precedents and the difficulties associated with our two-component models, we have applied a three-component model to the X-ray spectrum of NGC 3256, assuming that the absorption column density for the hard PL and warm R-S components is the same, and fixing the absorption column for the soft R-S component at the Galactic value. As indicated in Table 1, this model provides a slightly better fit to the *ASCA* spectra than the two-component models do (the improvement is significant at the 82% confidence level). The parameters derived for the three spectral components are, in some instances, poorly constrained, but their best-fit values are very similar to those we obtained for M82: for the hard power-law component, $\Gamma = 1.7$, for the warm thermal component, $kT = 0.8$ keV, and for the soft thermal component, $kT = 0.3$ keV. The column density for the hard and warm components is $N_{\rm H} = 8 \times 10^{21}$ cm^{-2}. As a free parameter, the column density for the soft component remains near the Galactic value at 1.0×10^{21} cm^{-2}. The three-component fit to the *ASCA* spectra is displayed in Figure 7*b*.

On statistical grounds, the two- and three-component models described above both provide acceptable fits to the *ASCA* spectrum of NGC 3256. As in the studies of M82 (Moran & Lehnert 1997) and NGC 4449 (Della Ceca et al. 1997), spatially resolved spectral information would help

[7] It is unlikely that the hard X-ray emission of starburst galaxies is dominated by extremely hot gas (see Suchkov et al. 1994); moreover, *ASCA* is not capable of measuring plasma temperatures that lie outside its energy range. Thus, we feel the (PL + R-S) form of the two-component model should be preferred.

us to eliminate one of the possibilities. Unfortunately, such information will not be available for NGC 3256 until the *Chandra X-ray Observatory* is deployed. But, in addition to our circumstantial objections to aspects of the two-component model, the success of the three-component model and its detailed similarity to the results obtained for starburst galaxies with similar attributes gives us confidence that it provides the more accurate description of the X-ray properties of NGC 3256. Therefore, we adopt that model for the remainder of this paper. It is important to note, however, that this choice does not significantly impact our assessment of the origin of the X-ray emission from NGC 3256. For example, the slope and normalization of the power law in the two- and three-component models are very similar; thus, our conclusions about the origin and intrinsic luminosity of this emission would be the same in either scenario. Likewise, the *total* intrinsic luminosity of the thermal emission from the galaxy, computed below in § 4.1, differs by less than 25% in the two- and three-component models.

4. Interpreting the X-Ray Spectrum of NGC 3256

Because our models for the broadband X-ray emission of NGC 3256 and M82 are so similar (cf. Moran & Lehnert 1997), we interpret their X-ray spectra in the same manner. We associate the warm and soft thermal components in the spectrum of NGC 3256 with the nuclear star formation and the starburst-driven wind, respectively. In § 4.2, we examine the properties of the hot gas and its relationship to the burst of star formation in NGC 3256. The origin of hard X-rays in the galaxy is less clear, and we consider several possibilities for the source of this emission in § 4.3. But first, now that we have an accurate model of its broadband X-ray spectrum, we reevaluate the luminosity of NGC 3256 in the X-ray band.

4.1. *The X-Ray Luminosity of NGC 3256*

The soft X-ray luminosities of starburst galaxies span several orders of magnitude up to a maximum of a few times $10^{41}\,\mathrm{ergs\,s^{-1}}$ (Fabbiano 1989). Thus, the 0.1–2.4 keV luminosity of $2 \times 10^{42}\,\mathrm{ergs\,s^{-1}}$, reported from the RASS by Boller et al. (1992), would appear to distinguish NGC 3256 as the most luminous X-ray starburst currently known. Although the RASS count rate of $0.113\,\mathrm{counts\,s^{-1}}$ for NGC 3256 listed in Boller et al. has been recently revised to $0.061\,\mathrm{counts\,s^{-1}}$ in the RASS Bright Source Catalogue (Voges et al. 1996), NGC 3256 remains, nonetheless, a bright X-ray source. But with an effective exposure of just 334 s (Voges et al. 1996), the RASS detection of NGC 3256 consists of only $\sim$ 20 counts—too few to provide detailed spectral information, a key ingredient for the accurate determination of the energy flux. The considerably more sensitive pointed X-ray observations described above provide this necessary spectral information.

Despite the fact that our PSPC spectrum of NGC 3256 contains just $\sim$ 230 counts, it does allow us to make a direct comparison to the RASS measurement since it was obtained with the same type of instrument used to conduct the RASS. The count rate derived from the pointed PSPC observation is $0.067\,\mathrm{counts\,s^{-1}}$, in agreement with the new RASS count rate reported by Voges et al. (1996). However, the spectral model used by Boller et al. (1992) to estimate the X-ray flux of NGC 3256—a power law with a photon index of 2.3—does not provide an acceptable fit to the PSPC spectrum ($\chi^2 = 33.5$ for 10 degrees of freedom). A model consisting of a $kT \approx 1$ keV Raymond-Smith thermal plasma, absorbed by the Galactic neutral hydrogen column density in the direction of NGC 3256, does a far superior job ($\chi^2 = 5.5$ for 9 degrees of freedom). Of course, this is not the correct form of NGC 3256's X-ray spectrum, but it describes the data in the 0.1–2.4 keV band and thus allows us to determine the flux in that band accurately. The fit with the Raymond-Smith model indicates an observed soft X-ray flux of $6.4 \times 10^{-13}\,\mathrm{ergs\,cm^{-2}\,s^{-1}}$ for NGC 3256. This translates to an unabsorbed luminosity of $4.2 \times 10^{41}\,\mathrm{ergs\,s^{-1}}$, a factor of five lower than the luminosity quoted by Boller et al. (1992).

However, our *ASCA* analysis has revealed the existence of significant internal absorption in NGC 3256, well in excess of the Galactic column density. The true soft X-ray luminosity of NGC 3256 should, therefore, be greater than that which we derived from the fit to the PSPC spectrum. In Table 2, we list the observed flux and intrinsic (unabsorbed) luminosity in various X-ray energy bands for each of the components in the three-component model. As expected, a higher value is obtained for the total intrinsic luminosity of NGC 3256 when the internal absorption is taken into account. Thus, we confirm that NGC 3256 is one of the most luminous X-ray starbursts known: in the 0.1–2.4 keV band, $L_{\rm X} = 1.9 \times 10^{42}$ ergs s^{-1}. (By a remarkable coincidence, this luminosity is nearly identical to the luminosity computed by Boller et al., which was determined using the wrong count rate and an inappropriate model.) In the following sections, we investigate in detail the origin of NGC 3256's copious X-ray emission.

4.2. *Nature of the Thermal X-ray Emission*

We have modeled the soft X-ray emission of NGC 3256 as two thermal plasmas, one with $kT \approx 0.3$ keV that is not absorbed above the Galactic column, and one with $kT \approx 0.8$ keV that is moderately absorbed ($N_{\rm H} \approx 10^{22}$ cm^{-2}). Conceptually, we associate the cooler of the two components with the spatially extended soft X-ray emission (seen in the *ROSAT* HRI image) from the hot, outflowing wind described in § 2.1. The absorption and strong emission lines associated with the warm $kT = 0.8$ keV plasma suggest that this component arises from supernova remnants and supernova-heated gas within a much smaller volume near the starburst nucleus. Because of the limitations of the X-ray instrumentation at our disposal and the modest signal to noise ratio of our spectra of NGC 3256, the true nature of the thermally emitting gas in the galaxy may actually be more complex. Nonetheless, the characteristics of the hot gas in NGC 3256 are intimately linked to the star formation in the galaxy, and it is instructive to examine whether the physical parameters we infer for the thermal X-ray–emitting gas are consistent with other observed and predicted properties of the starburst.

4.2.1. Physical Parameters of the "Soft" X-ray–Emitting Gas

The normalization of the "soft" 0.3 keV thermal plasma in the three-component model listed in Table 1 implies a value for the emission integral $EI = \int n_e^2 \, dV$ of 4.1×10^{63} cm^{-3}. Assuming that the emission associated with this plasma is uniformly distributed over a spherical region 6 kpc in radius (corresponding to the extent of the soft X-ray emission we observe), we derive a total volume for the emitting region of $V = 2.6 \times 10^{67}$ cm^3. In terms of a volume-filling factor $f_{\rm s}$ for this gas, we compute the following physical parameters for the soft thermal plasma: the gas density $n_e = (EI/Vf_{\rm s})^{1/2} = 1.3 \times 10^{-2} \, f_{\rm s}^{-1/2}$ cm^{-3}, the gas pressure $P_{\rm X} \approx 2 n_e kT = 1.2 \times 10^{-11} \, f_{\rm s}^{-1/2}$ dyne cm^{-2}, the mass $M_{\rm X} \approx n_e m_{\rm p} V f_{\rm s} = 2.7 \times 10^8 \, f_{\rm s}^{1/2} \; M_\odot$, and the total thermal energy $E_{\rm X} \approx 3 n_e kTV f_{\rm s} = 4.6 \times 10^{56} \, f_{\rm s}^{1/2}$ ergs. Using the emissivity of a 0.3 keV gas with solar abundances $\Lambda = 3.3 \times 10^{-23}$ ergs cm^3 s^{-1} (Sutherland & Dopita 1993), we calculate a radiative cooling time $t_{\rm cool} \approx 3kT/(\Lambda n_e) = 1.1 \times 10^8 \, f_{\rm s}^{1/2}$ yr.

Heckman et al. (1990) have measured the density and pressure of the optical emission-line gas in NGC 3256 (via the [S II] λ6716/ [S II] λ6731 ratio) as a function of distance from the nucleus. If this gas were in pressure equilibrium with the X-ray plasma, we would have a means for estimating the X-ray volume-filling factor $f_{\rm s}$. However, the total pressure of the optical line-emitting gas may be dominated not by its thermal pressure, but by the ram pressure of the outflowing wind. Thus, equating the above relation for the pressure of the X-ray plasma $P_{\rm X}$ with the (total) pressure of the emission-line gas $P_{\rm opt}$ affords, strictly speaking, a lower bound on $f_{\rm s}$, which is useful nonetheless. At a projected distance of 6 kpc from the nucleus, the Heckman et al. density profile indicates $P_{\rm opt} \approx 1.4 \times 10^{-10}$ dyne cm^{-2}, which implies $f_{\rm s} \geq 0.01$. Using this limit for $f_{\rm s}$ in the above expressions, we have $n_e \leq 0.13$ cm^{-3}, $M_{\rm X} \geq 2.7 \times 10^7 \; M_\odot$, $E_{\rm X} \geq 4.6 \times 10^{55}$ ergs, and

$t_{\rm cool} \geq 1.1 \times 10^7$ yr. The cooling time is comparable to the sound crossing time of $\sim 2 \times 10^7$ yr expected for the 0.3 keV plasma.

4.2.2. Physical Parameters of the "Warm" X-ray–Emitting Gas

The normalization of the "warm" 0.8 keV thermal plasma in the three-component model yields an emission integral $EI = 4.9 \times 10^{64}$ cm^{-3}. Unfortunately, our X-ray data do not directly constrain the size of the region occupied by this plasma. However, we have spectral evidence that the X-ray emission originates near the nucleus (inferred from the considerable absorption found for this component in our fit) and that it is associated with supernova remnants, suggesting that the 0.8 keV gas is distributed over the volume within which the bulk of the star formation is occurring. This is also the region of mass and energy injection, which, based on the pressure profile of the optical emission-line gas, has an estimated radius of $\sim$ 1.4 kpc (adjusted for the distance we have adopted for NGC 3256; Heckman et al. 1990). Assuming spherical geometry, we calculate the volume of the region responsible for the 0.8 keV thermal emission to be 3.4×10^{65} cm^3, which suggests a pressure for the warm X-ray plasma (in terms of a volume-filling factor $f_{\rm w}$) of $P_{\rm X} = 1.0 \times 10^{-9} f_{\rm w}^{-1/2}$ dyne cm^{-2}. As in the previous section, we can equate this expression for $P_{\rm X}$ with the pressure of the optical emission-line gas $P_{\rm opt}$ to obtain a lower limit for $f_{\rm w}$. At a distance of 1.4 kpc from the nucleus of NGC 3256, $P_{\rm opt} \approx 2 \times 10^{-9}$ dyne cm^{-2} (Heckman et al. 1990), which implies $f_{\rm w} \geq 0.25$. Thus, for the warm X-ray–emitting gas, we derive the following physical parameters: $n_e \leq 0.8$ cm^{-3}, $M_{\rm X} \geq 5.4 \times 10^7$ $M_\odot$, $E_{\rm X} \geq 2.5 \times 10^{56}$ ergs, and, using a value of 2.7×10^{-23} ergs cm^3 s^{-1} for the emissivity of a 0.8 keV plasma with solar abundances (Sutherland & Dopita 1993), $t_{\rm cool} \geq 5.9 \times 10^6$ yr. Again, the cooling time is comparable to the sound crossing time of $\sim 3 \times 10^6$ yr expected for this component.

4.2.3. Powering the Thermal X-ray Emission

Based on the preceding analysis, we estimate the overall mass and energy of the X-ray–emitting gas in NGC 3256 to be $M_{\rm X} \geq 8.1 \times 10^7$ $M_\odot$ and $E_{\rm X} \geq 3.0 \times 10^{56}$ ergs. As indicated in Table 2, the luminosity of this gas in the 0.1–10 keV band is $L_{\rm X} = 1.8 \times 10^{42}$ ergs s^{-1}. We can compare these quantities to the results of starburst models (e.g., Leitherer, Robert, & Drissen 1992; Leitherer & Heckman 1995), which predict the *total* amount of mass and mechanical energy deposited into the interstellar medium (ISM) by the burst of star formation. These models are calculated as a function of the age of the starburst for the following parameters: the slope α and upper mass limit $M_{\rm upp}$ of the stellar mass function, and the metallicity of the star-forming region Z. The set of parameters considered by Leitherer & Heckman (1995) that most closely matches the conditions in NGC 3256 are: $\alpha = 2.35$, $M_{\rm upp} = 100$ $M_\odot$ (Rigopoulou et al. 1996), and $Z = Z_\odot$ (§ 2.3). Assuming that star formation has been approximately constant over a period of $\sim 2 \times 10^7$ yr (Rigopoulou et al. 1996), these parameters imply a bolometric absolute magnitude $M_{\rm bol} = -20.60$ for a star-formation rate of 1 $M_\odot$ yr^{-1} (Leitherer & Heckman 1995), which corresponds to a bolometric luminosity of $L_{\rm bol} = 1.4 \times 10^{10}$ $L_\odot$ $(M_\odot$ yr$^{-1})^{-1}$. Since the majority of the bolometric luminosity of NGC 3256 is emitted in the far infrared, the FIR luminosity of $L_{\rm FIR} = 6 \times 10^{11}$ $L_\odot$ suggests a star-formation rate of ~ 40 $M_\odot$ yr^{-1}. For this star-formation rate, the Leitherer & Heckman models predict that $M_{\rm total} = 1 \times 10^8$ $M_\odot$ and $E_{\rm total} = 7 \times 10^{57}$ ergs have been released into the galaxy's ISM over the lifetime of the starburst, and that kinetic energy is being injected into the ISM at a rate of 2×10^{43} ergs s^{-1}. The relevant time scale for a comparison of the mechanical energy output of the starburst and the current thermal energy of the X-ray plasmas is the gas outflow time, which is approximately equivalent to the sound crossing time of the warm X-ray plasma. On this time scale (a few Myr), the starburst injects $E_{\rm X} \approx 10^{57}$ ergs into the ISM. Thus, in light of the values of $M_{\rm X}$, $E_{\rm X}$, and $L_{\rm X}$ listed above for the X-ray plasmas, it would appear that the starburst in NGC 3256 is indeed capable of powering the observed thermal X-ray emission.

According to the theory of starburst-driven superwinds, the softest X-ray emission we observe arises from clouds that are shock-heated by the hot, outflowing wind material, rather than from the wind itself or supernova ejecta (Suchkov et al. 1994, and references therein). Thus, there should be a direct relationship between the rate at which stellar winds and supernovae are injecting energy into the galaxy and the rate at which the ambient interstellar medium is being shock-heated. Assuming (1) that mechanical energy is being deposited into the ISM of NGC 3256 at a rate of $L_{\rm mech} = 2 \times 10^{43}\,{\rm ergs\,s^{-1}}$, (2) that the temperature of the injected wind material is equivalent to that of the warm thermal component in our spectral model ($kT = 0.8$ keV), and (3) that energy is conserved between the warm and soft thermal plasmas, we derive a mass-heating rate of $\dot{M}_{\rm heat} = (L_{\rm mech} m_p)/(3kT) \approx 140\ M_\odot\ {\rm yr^{-1}}$. The Leitherer & Heckman models, on the other hand, predict that the starburst injects just $\sim 10\ M_\odot\ {\rm yr^{-1}}$ into the galaxy's ISM, which implies that the wind in NGC 3256 must be heavily "mass-loaded" (Suchkov et al. 1994, 1996; see also Della Ceca et al. 1997). The temperature of the injected wind material may in fact be higher than we have assumed it to be. If so, the amount of mass loading would be proportionally lower. Nonetheless, the likelihood that the wind of NGC 3256 is mass-loaded suggests that heavy-element abundances in the soft thermal plasma are similar to those of the ambient interstellar gas in the galaxy's nuclear region, which we have demonstrated are approximately solar (§2.3). This substantiates our adoption of solar abudances for this component in our model of the X-ray spectrum of NGC 3256.

4.3. *Sources of Hard X-Ray Emission in NGC 3256*

Observations in the 2–20 keV band with the *Ginga* satellite first revealed that star-forming galaxies, as a class, are emitters of hard X-rays (Ohashi & Tsuru 1992). *ASCA* now provides the opportunity to disentangle the complex X-ray spectra of these objects and to determine the energetic processes responsible for their high-energy emission. An understanding of the hard X-ray properties of starburst galaxies will lead to a more complete physical description of the starburst phenomenon and will permit us to evaluate the contribution of these objects to the cosmic X-ray background. In this section we consider sources of hard (> 2 keV) X-rays likely to be associated with the starburst in NGC 3256—accretion-powered binaries and inverse-Compton scattered emission—as well as the possibility that the galaxy's hard X-ray emission is produced instead by a hidden Seyfert nucleus.

4.3.1. An Obscured Active Nucleus

As we demonstrated in § 4.1, the total X-ray luminosity of NGC 3256 is high for a starburst galaxy. In addition, the best-fit slope of the power-law component we derive (energy index $\alpha_{\rm X} = 0.7$) is similar to the slope of a typical Seyfert galaxy X-ray spectrum (Nandra & Pounds 1994). The amount of absorption applied to this component in our fit ($N_{\rm H} \approx 10^{22}\ {\rm cm^{-2}}$) could be interpreted as evidence that NGC 3256 contains an obscured low-luminosity Seyfert nucleus. Based on the IR brightness of NGC 3256 ($L_{\rm FIR} = 6 \times 10^{11}\ L_\odot$) and the popularity of an evolutionary scenario linking ultraluminous IR galaxies to the origin of quasars (Sanders et al. 1988), several authors have addressed the question of whether or not NGC 3256 harbors a buried AGN. But observations in the near-infrared (Moorwood & Oliva 1994; Kotilainen et al. 1996), radio (Norris & Forbes 1995), and optical (§ 2) bands have *all* failed to indicate Seyfert activity in NGC 3256. Mid-infrared spectroscopy obtained with the *Infrared Space Observatory (ISO)*, which can penetrate obscuration equivalent to $A_V \approx 50$ mag, has provided the most compelling evidence to date that the burst of star formation in NGC 3256—*not* a buried active nucleus—powers the galaxy's luminosity. High-excitation emission lines, such as [O IV] 25.9μ and [Ne V] 14.3μ, which are indicative of photoionization by a hard, nonstellar continuum, were not detected in the *ISO* spectrum of NGC 3256 (Rigopoulou et al. 1996). Instead, photoionization by hot stars provides a fully adequate explanation for the IR emission-line properties of the galaxy (Lutz et al. 1996). Given the absence

of any evidence for an AGN in NGC 3256, we are reluctant to invoke a buried Seyfert nucleus to explain the galaxy's hard X-ray emission.

4.3.2. X-ray Binaries

The identification of high-mass X-ray binary star systems (HMXBs) in the Galaxy and Magellanic Clouds has led to the expectation that such sources contribute significantly to the total X-ray emission of other star-forming galaxies (Fabbiano 1989). Since HMXBs have distinctly flat X-ray spectra below 10 keV ($\bar{\Gamma} \approx 1.2$; White, Swank, & Holt 1983; Nagase 1989), the energy range and resolution afforded by *ASCA* should permit a sensitive spectral test of this hypothesis. Yet despite *ASCA*'s capabilities, the role of HMXBs in starburst galaxies remains unclear. While the hard X-ray spectra of some starbursts may be consistent with those of Galactic HMXBs (Yaqoob et al. 1995; Awaki et al. 1996), the spectra of other objects clearly are not (Moran & Lehnert 1997; Della Ceca et al. 1996, 1997; Ptak et al. 1997). Unfortunately, the constraints we have derived here for the slope of the hard component in the X-ray spectrum of NGC 3256 are insufficient for a meaningful comparison to the spectra of HMXBs. Thus, we must consider the contribution of HMXBs to the energy budget of NGC 3256 instead.

HMXBs consist of an early-type star and the compact remnant of an early-type star. Therefore, the number of O stars in a star-forming region should provide an indication of the number of HMXBs present. If the star-formation rate is approximately constant, O star births and deaths will reach equilibrium in $\sim 10^7$ yr, after which time the number of O stars will remain constant (Leitherer & Heckman 1995). Since the duration of the X-ray–emitting phase of a high-mass binary system is much shorter than the lifetimes of even the most massive stars (e.g., Dalton & Sarazin 1995), the HMXB population will also reach equilibrium on this time scale. Thus, under these conditions, the number of HMXBs in a star-forming region should be directly proportional to the number of O stars present, regardless of the star-formation rate.

To determine the number of O stars in the nucleus of NGC 3256, we have employed the method of Vacca (1994), which requires an estimate of Q, the number of ionizing photons (i.e., those with $\lambda < 912$ Å) emitted per second by O stars. Based on the *ISO* observation of NGC 3256 (Rigopoulou et al. 1996), Lutz et al. (1996) computed a Lyman continuum luminosity of 2.9×10^{10} $L_\odot$, which, after adjustment for a distance of 56 Mpc and their adopted mean photon energy of 15 eV, corresponds to $Q = 1.0 \times 10^{55}$ photons s^{-1}. If we assume solar metallicity for the star-forming region ($Z \approx Z_\odot$; § 2) and a stellar upper mass cutoff $M_{\rm upp}$ of 80–100 $M_\odot$ (Rigopoulou et al. 1996), and allow for a range of possible values of the slope of the initial mass function α = 2.0–2.7, we estimate that there are between 7.0×10^5 and 1.3×10^6 O stars in the starburst nucleus of NGC 3256. This is consistent with the value of 1.0×10^6 O stars predicted by Leitherer & Heckman (1995) for a constant star-formation rate of 40 $M_\odot$ yr^{-1}, $\alpha = 2.35$, $M_{\rm upp} = 100$ $M_\odot$, $Z = Z_\odot$, and a starburst age of $> 10^7$ yr. As indicated in Table 2, the 2–10 keV luminosity of the power-law component in the spectrum of NGC 3256 is 1.9×10^{41} ergs s^{-1}. Given the number of O stars calculated here, we require a specific hard X-ray luminosity for NGC 3256 of (1.5–2.7) $\times$ 10^{35} ergs s^{-1} per O star.

This value is substantially in excess of that found in the Milky Way, an appropriate system for comparison given the solar abundance we measure in NGC 3256. When calculating the specific hard X-ray luminosity per O star, it is essential to define with care the X-ray luminosity of each contributing HMXB system. All such X-ray sources are variable; indeed, the vast majority of HMXBs by number are the Be star X-ray binaries, which have very small duty cycles and very low quiescent X-ray luminosities. Furthermore, catalogued fluxes for HMXB systems are quoted for a variety of different observing bands and assumed spectral forms, and often include only the maximum flux ever observed, or the maximum and minimum recorded fluxes (where the latter is usually an upper limit) and no duty cycle information (cf. Bradt & McClintock 1983; van Paradijs 1995). While these data are sufficient for most applications, they do not allow a determination of

the *time-averaged* source luminosity required for a calculation of the specific X-ray luminosity per O star.

To address this issue, we have carried out an extensive review of the literature and various data archives, from which we have assembled a volume-limited sample of nearly 60 HMXBs within 3.5 kpc of the Sun. Using the available all-sky-monitor databases, we have determined the mean 2–10 keV luminosity of each source in this list (Helfand & Moran 1999). In conjunction with the comprehensive new catalog of OB stars in the solar neighborhood compiled by C. Garmany (1998, private communication), this provides a firm upper limit on the specific luminosity of 4×10^{34} ergs s^{-1} per O star; the best estimate is a factor of two lower. These values are consistent with that obtained for the Galaxy as a whole using the HMXB population syntheses of Portegies Zwart & Verbunt (1996) and Dalton & Sarazin (1995). Thus, we conclude that less than $\sim 20\%$ of the hard X-ray emission from NGC 3256 arises from its HMXB population.

4.3.3. Inverse-Compton Scattering

Inverse-Compton scattering (IC), involving the interaction of infrared photons with supernova-generated relativistic electrons, was among the first mechanisms proposed to explain the emission of hard X-rays from M82 (Hargrave 1974). Although the IC hypothesis is difficult to test, the luminosities of M82's cospatial mid-infrared and nonthermal radio sources indicate that the IR photons and relativistic electrons possess energy densities high enough for the production of a significant X-ray flux through the IC process (Rieke et al. 1980). Observations of the broadband X-ray spectrum and luminosity of M82 have pointed to IC emission as an important source of X-rays at energies above a few keV (Schaaf et al. 1989; Moran & Lehnert 1997). The nuclear region of NGC 3256 is also a luminous source of infrared and radio emission. Given the shortcomings of other explanations for its hard X-ray flux, the role of IC scattering in NGC 3256 should be explored as well.

The calculation of the expected IC X-ray luminosity depends on the geometry adopted for the emitting region, which can only be approximated for an object as distant as NGC 3256. Fortunately, some assistance is provided by recent high-resolution radio (Norris & Forbes 1995) and near-IR (Kotilainen et al. 1996) images of NGC 3256. These have revealed the presence of two resolved nuclei in the galaxy separated by $\sim 5''$. The 5 GHz flux densities of the nuclei are nearly identical (34 mJy and 31 mJy), as are their radio spectral indices ($\alpha_{\rm r} = 0.78$ and 0.86 for $S_\nu \propto \nu^{-\alpha_{\rm r}}$). For simplicity, therefore, we will assume that $S_5 = 33$ mJy and $\alpha_{\rm r} = 0.8$ for each nucleus, and that each is responsible for half of the galaxy's infrared luminosity of 2.4×10^{45} ergs s^{-1}. Assuming further that the nuclei are spherical, their measured radio sizes ($1\farcs2$ FWHM; Norris & Forbes 1995) imply they have radii of $0\farcs7$ (190 pc).

If the relativistic electrons and inverse-Compton seed photons are cospatial with a uniform magnetic field B, the IC luminosity can be expressed as $L_{\rm IC} = L_{\rm synch} \times (U_{\rm ph}/U_{\rm B})$, where $L_{\rm synch}$ is the total synchrotron luminosity produced by the electrons, $U_{\rm ph}$ is the energy density of the seed photon field, and $U_{\rm B}$ is the energy density of the magnetic field. Integration of the radio spectrum of NGC 3256 between 10 MHz and 200 GHz yields $L_{\rm synch} = 5.7 \times 10^{39}$ ergs s^{-1} for each nucleus. For a spherical region of radius r, the seed photon energy density is given by $U_{\rm ph} = 3L_{\rm bol}/4\pi r^2 c$, where $L_{\rm bol}$ is the bolometric luminosity of the region and c is the speed of light. In NGC 3256, $L_{\rm bol} \approx L_{\rm FIR}$, implying $U_{\rm ph} = 2.8 \times 10^{-8}$ ergs cm^{-3} in each nucleus. An estimate of $U_{\rm B}$ can be derived under the assumption that the minimum energy condition obtains in the synchrotron-emitting plasma. From equation (2) of Miley (1980), we calculate a minimum energy magnetic field strength of $B_{\rm min} = 70\ (1+k)^{2/7}\ \mu$G. Here k is the proton-electron energy ratio, which, although unmeasured, is thought to lie between 1 and 100. For this range of k, $U_{\rm B}$ $(= B_{\rm min}^2/8\pi)$ has a value of 2.9×10^{-10} to 2.7×10^{-9} ergs cm^{-3}. The combined IC luminosity of both nuclei, integrated over the entire range of upscattered energies, is therefore expected to be between 1.2×10^{41} ergs s^{-1} and

1.1×10^{42} ergs s^{-1}, suggesting that IC scattering may indeed account for a significant fraction of the hard X-ray emission of NGC 3256.

To compute the IC luminosity emitted in the *ASCA* band, we employ the approach described by Tucker (1975). This method capitalizes on the fact that electrons possessing a power-law distribution of energies with index n produce power-law synchrotron and IC spectra with identical energy indices $\alpha = (n-1)/2$. (Note that the hard X-ray and nuclear radio spectra of NGC 3256 *do* have approximately the same slopes.) Assuming the seed photon field has a blackbody spectrum of temperature T, the ratio of the IC and synchrotron spectral power per unit volume can be expressed as

$$K = 2.47 \times 10^{-19}\ (5.25 \times 10^3)^{\alpha}\ T^{3+\alpha}\ B^{-(1+\alpha)}\ b(n)/a(n)\ . \tag{1}$$

The value of 0.8 we have adopted here for α implies $n = 2.6$, which corresponds to values of 0.08 and 8.4 for the dimensionless functions $a(n)$ and $b(n)$, respectively. The observed 60 μm to 100 μm *IRAS* flux density ratio for NGC 3256 ($S_{60}/S_{100} = 0.77$) suggests a dust temperature of $T = 44.4$ K (assuming a modified blackbody in which the dust emissivity is proportional to the frequency ν; see Helou et al. 1988). Thus, for the range of $B_{\rm min}$ derived above, $K = 0.13$–0.95.

The quantity K can then be used to relate the expected IC flux density $F_{\rm IC}$ at an X-ray frequency $\nu_{\rm IC}$ to the observed synchrotron flux density $F_{\rm s}$ at a radio frequency $\nu_{\rm s}$:

$$K = (F_{\rm IC}/F_{\rm s}) \times (\nu_{\rm IC}/\nu_{\rm s})^{\alpha}\ . \tag{2}$$

Using the total nuclear 5 GHz radio flux density of NGC 3256, we compute an expected 5 keV IC flux density of $(0.4 - 3.0) \times 10^{-14}$ ergs cm^{-2} s^{-1} keV^{-1}. Comparison to the observed 5 keV flux density of NGC 3256 of $\sim 6.4 \times 10^{-14}$ ergs cm^{-2} s^{-1} keV^{-1} (see the lower panel of Fig. 7b) suggests that IC scattered emission accounts for 6–47% of the hard X-ray flux in the *ASCA* bandpass.

Given the value for the binary contribution obtained above ($< 20\%$), it would appear that our simple estimate yields an IC flux that still falls short of the total measured hard X-ray flux from NGC 3256. However, it is important to bear in mind that the IC calculation is highly idealized: we have assumed that (1) the geometry of the starburst region is simple, (2) the electron, photon, and magnetic field energy densities are uniform, and (3) the minimum energy scenario is valid. Deviations from these conditions could have a significant impact on the actual IC luminosity produced. For instance, a substantially higher IC flux would result if the ambient magnetic field strength were slightly below the equipartition value. In addition, the spatial distribution of the relativistic electrons and infrared photons may be knotty, amplifying the local electron and photon energy densities in some fraction of the star-forming region. In light of these uncertainties, it is possible that the role of IC scattering in NGC 3256 may be more significant than our calculations above would suggest. High-resolution radio, infrared, and hard X-ray observations are needed to improve our understanding of the importance of IC scattering in this and other starburst nuclei.

5. Starburst Galaxies and the X-ray Background

Perhaps the most pressing unsolved problem in extragalactic X-ray astronomy is the origin of the cosmic X-ray background (XRB). It is now known that the XRB above ~ 1 keV is produced by discrete emitters rather than arising in a truly diffuse medium (Mather et al. 1990; Wright et al. 1994). But despite vigorous attempts, efforts to resolve the XRB completely have not yet succeeded. In an extremely deep *ROSAT* survey, approximately 70% of the 1–2 keV XRB was resolved into discrete sources (Hasinger et al. 1998). Follow-up optical spectroscopy has revealed that, as in shallower soft X-ray surveys, the majority of these sources are high-luminosity active galactic nuclei (Schmidt et al. 1998). Paradoxically, the broadband X-ray spectra of such sources are considerably steeper than the spectrum of the XRB itself (e.g., Nandra & Pounds 1994); thus, the objects that dominate the XRB in the soft band contribute only a small fraction of the background

at higher X-ray energies (Fabian & Barcons 1992). It remains unclear (1) what population is responsible for the as-yet unresolved soft XRB, and (2) if these sources, once identified, will exhibit the spectral properties required to account for the overall shape of the XRB spectrum.

Although it is currently fashionable to attribute the balance of the XRB radiation to a population of intrinsically absorbed Seyfert galaxies (e.g., Madau, Ghisellini, & Fabian 1994; Comastri et al. 1995), it has been proposed on a number of occasions that starburst galaxies might also make a significant contribution to the XRB (Bookbinder et al. 1980; Stewart et al. 1982; Weedman 1987; Griffiths & Padovani 1990; Rephaeli et al. 1991; David et al. 1992). The emission of hard X-rays appears to be ubiquitous among starbursts; therefore, their integrated contribution could rival that of classical AGNs, which, despite being more luminous, are considerably more rare. Previously, it has been assumed that HMXBs dominate the emission of star-forming galaxies above a few keV (e.g., Bookbinder et al. 1980; Griffiths & Padovani 1990). In our investigations, we have concluded that inverse-Compton scattering provides an equally plausible explanation for the hard X-ray luminosities of both NGC 3256 (§ 4) and M82 (Moran & Lehnert 1997). Independent of the emission mechanism, however, we can use these new measurements of the hard X-ray flux from starbursts to estimate the contribution such galaxies make to the XRB.

A key aspect of any such calculation is the assumption concerning the evolution of the starburst galaxy population with cosmic time. Rather than attempt to model this evolution, we seek an observational contraint on the total number of potential contributors. It has long been established that there exists a very tight correlation between the far-infrared emission of (non-AGN) galaxies and their centimetric radio flux densities (Helou, Soifer, & Rowan-Robinson 1985). While a detailed physical explanation for this correlation is not yet in hand, it is apparent that star-formation is responsible for generating the bulk of the radiation in both bands—in the far infrared from stellar UV radiation reprocessed by dust, and in the radio from H II region free-free emission plus synchrotron radiation generated by the relativistic electrons accelerated in supernova explosions. Thus, the 5 GHz radio emission from galaxies lacking a radio-loud AGN can be used as a surrogate for estimating their star formation activity.

Since current sensitivities in both the far-IR and X-ray bands are insufficient to probe star forming populations directly at intermediate and high redshifts, we base our analysis on the well-constrained radio source counts. Below a flux density of $\sim$ 1 mJy, the radio source population is associated predominantly with faint, blue (and presumably star-forming) galaxies, rather than with quasars and early-type galaxies, which account for the majority of sources at higher flux densities (e.g., Windhorst et al. 1985; Kron, Koo, & Windhorst 1985; Thuan & Condon 1987; Condon 1989; Benn et al. 1993; Windhorst et al. 1995; Richards et al. 1998). The 5 GHz number count–flux relation ($\log N - \log S$) measured by Fomalont et al. (1991) thus provides the means by which we can estimate the integrated contribution of starburst galaxies to the XRB. Over a flux density range of 16 μJy to 1 mJy, Fomalont et al. found that, for S in units of μJy, $N(>S) = 23.2\ S^{-1.2}$ arcmin^{-2}. On the basis of fluctuation statistics, they showed further that the relation continues with approximately the same slope down to $\sim$ 2 μJy. In differential form, the microjansky number counts can thus be expressed as $n(S) = -27.8\ S^{-2.2}$ arcmin^{-2} $= -1.0 \times 10^5\ S^{-2.2}$ deg^{-2}. Provided we can relate the expected X-ray emission from a galaxy directly to its radio flux density, the following equation then describes the contribution of starburst galaxies to the intensity of the XRB:

$$I_{\rm X} = \int n(S)\ f_{\rm SB}(S)\ F_{\rm X}(S)\ dS \tag{3}$$

where $f_{\rm SB}(S)$ is the fraction of radio sources with a 5 GHz flux density of S that are starburst galaxies, and $F_{\rm X}(S)$ is the X-ray flux.

As we have discussed above, IC emission in starburst galaxies provides a direct connection between their radio and X-ray emission; however, since it depends in part on the geometry of the star-forming region, it is not obvious that this emission will scale linearly with the radio flux density.

Alternatively, if HMXBs and/or supernova remnants produce the bulk of the hard X-ray emission, the link between radio flux density and X-ray output may be even less direct. Nonetheless, in both starburst galaxies for which we have a good measurement of the hard X-ray flux, $R_{5,5}$, the ratio of the 5 keV flux density[8] to the *core* 5 GHz flux density, has approximately the same value. In NGC 3256, the 5 keV flux density is 6.4×10^{-14} ergs cm^{-2} s^{-1} keV^{-1} and the core 5 GHz flux density is 65 mJy (Norris & Forbes 1995). In M82, the 5 keV flux density is 3.2×10^{-12} ergs cm^{-2} s^{-1} keV^{-1} (Moran & Lehnert 1997) and the core 5 GHz radio flux density is 3.4 Jy (Hargrave 1974). Thus, for both galaxies $R_{5,5} \approx 10^{-18}$ ergs cm^{-2} s^{-1} keV^{-1} μJy^{-1}.

In the IC picture, the hard X-ray and GHz radio spectra of starburst galaxies are expected to have the same slope, so $R_{5,5}$ does not need to be adjusted for redshift effects (in other scenarios, a K-correction may be required). We do, however, need to account for the fact that only a fraction $f_{\rm core}$ of the total observed radio flux of a starburst galaxy is emitted in the nuclear region. In M82, $f_{\rm core} = 0.85$ (Hargrave 1974), which we will adopt as typical for starburst galaxies. Thus, for a given *total* 5 GHz flux density S, we estimate the expected 5 keV flux density as $F_{5\ {\rm keV}} = R_{5,5}\ f_{\rm core}\ S$ ergs cm^{-2} s^{-1} keV^{-1}; equation (3) then becomes

$$I_{5\ {\rm keV}} = -1.0 \times 10^5 \int R_{5,5}\ f_{\rm core}\ f_{\rm SB}(S)\ S^{-1.2}\ dS\ . \tag{4}$$

Assuming, for the time being, that $f_{\rm SB}$ does not vary with S, evaluation of the integral yields

$$I_{5\ {\rm keV}} = 4.3 \times 10^{-13}\ f_{\rm SB}\ \left[{S_1}^{-0.2} - {S_2}^{-0.2}\right]\ {\rm ergs\ cm^{-2}\ s^{-1}\ keV^{-1}\ deg^{-2}} \tag{5}$$

where S_1 and S_2 are, respectively, the lower and upper limits of integration, in units of μJy.

The change in the slope of the radio $\log N - \log S$ relation, below which radio sources become associated with faint blue galaxies, occurs somewhere in the neighborhood of one to a few mJy (Fomalont et al. 1991, and references therein). For the power-law form of this relation used in equation (4), sources with fluxes in excess of these values make virtually no contribution to the integral, so we may take S_2 to be infinity. Our estimate of $I_{5\ {\rm keV}}$ depends, therefore, entirely on the value we adopt for S_1. Windhorst et al. (1993) have shown that the radio source counts at 8.3 GHz must converge below 20 nJy; otherwise, discrete radio sources would distort the cosmic microwave background spectrum at centimeter wavelengths. The corresponding limit for 5 GHz sources, if we apply the mean spectral index of -0.35 measured by Windhorst et al. (1993) for sources in the microjansky regime, is 24 nJy. Thus, assuming $f_{\rm SB} \approx 1$ (which could well be appropriate for sub-μJy sources) and $S_1 = 0.024\ \mu$Jy, equation (5) yields $I_{5\ {\rm keV}} = 9.1 \times 10^{-13}$ ergs cm^{-2} s^{-1} keV^{-1} deg^{-2}. Comparing this value to the measured intensity of the XRB at 5 keV of 2×10^{-12} ergs cm^{-2} s^{-1} keV^{-1} deg^{-2} (Gendreau et al. 1995), we find that star-forming galaxies may contribute as much as 45% of the 5 keV XRB.

Analysis of optical galaxy counts (Windhorst et al. 1993) and the far-infrared background (Haarsma & Partridge 1998) have suggested that the radio source population may dwindle at fluxes as high as 0.3–1 μJy. In addition, optical identifications of 10–1000 μJy radio sources indicate that only $\sim$ 70% to 80% are likely to be associated with star-forming galaxies (Windhorst et al. 1995; Richards 1998). Thus, if we conservatively assume that $S_1 = 1\ \mu$Jy and $f_{\rm SB} = 0.75$, equation (5) yields $I_{5\ {\rm keV}} = 3.2 \times 10^{-13}$ ergs cm^{-2} s^{-1} keV^{-1} deg^{-2}, equivalent to $\sim$ 15% of the 5 keV XRB.

The Cosmic Infrared Background (CIB), recently measured from an analysis of the *COBE* satellite data (Dwek et al. 1998, and references therein), provides another constraint on the fraction of the background in any band contributed by processes associated with star formation. The energy

[8] An X-ray energy of 5 keV is ideal for this calculation: the 5 keV flux densities of starburst galaxies observed with *ASCA* are relatively well determined, and they are unaffected by modest photoelectric absorption or the soft thermal emission components which dominate at lower energies.

density of the CIB in the 125 μm to 5000 μm band is $(6.7 \pm 1.7) \times 10^{-15}$ ergs cm^{-3} (from Dwek et al. 1998), while between 5 and 35 keV, the band for which a new population of flat-spectrum XRB contributors is required, the observed energy density is $\sim 3.5 \times 10^{-17}$ ergs cm^{-3}. This implies that only $\sim 10^{-3}$ of the CIB radiation needs to be processed into hard X-rays in order to make a 25% contribution to the XRB flux. The far-infrared–to–X-ray luminosity ratio for NGC 3256 is $\sim 2 \times 10^{-4}$; thus, if all starbursts contribute at this level, the overall background contribution would be $\sim 5\%$. It is not difficult to imagine evolutionary effects (in the IMF slope, the compactness of the nuclear starbursts, the metallicity, etc.) that would raise this contribution considerably. Furthermore, Steidel et al. (1999) have recently shown that star formation activity in galaxies at $\langle z \rangle \approx 4.1$ is significant, with very modest levels of obscuration by dust; such UV/visible emitters would not contribute significantly to the CIB, but could well contribute to the XRB an amount comparable to dust-enshrouded star-forming regions. Since the optical/UV background light is roughly equal in energy density to the CIB, the contribution to the XRB by star formation could increase by an additional factor of ~ 2.

A number of issues must be investigated further in order to refine our estimate of the contribution star-forming galaxies make to the XRB. First, we require a better understanding of the relationship between the radio and hard X-ray properties of starburst galaxies. A definitive determination of the origin of their hard X-ray emission would facilitate this understanding. Second, the function $f_{\rm SB}(S)$ needs to be determined through optical identification programs for the faintest known radio sources (e.g., Richards 1998). Finally, the nature of the radio $\log N - \log S$ relation below $S \approx 1$ μJy is of crucial importance, since a major fraction of the XRB contribution of starbursts could arise from sub-μJy sources.

It remains to be seen whether the average X-ray spectra of distant star-forming galaxies are flat enough to help resolve the XRB spectral paradox—that all identified constributors have spectra steeper than that of the integrated background itself. However, indications from the microjansky radio source statistics are encouraging in this regard. Windhorst et al. (1993) have demonstrated that the spectra of microjansky radio sources, most of which are likely to be star-forming galaxies, flatten to $\bar{\alpha}_{\rm r} = 0.35 \pm 0.15$ at the faintest measured flux densities. This is consistent with both the slope of the XRB spectrum of $\alpha_{\rm X} = 0.41 \pm 0.03$ measured by Gendreau et al. (1995) and the IC model requirement that the radio and X-ray spectral slopes be the same. Such a hypothesis is easily testable: a 500 ks *Chandra* pointing would be able to detect NGC 3256 to $z = 2$, and will contain dozens of starburst galaxies coincident with radio sources brighter than ~ 10 μJy if the IC radiation from starbursts produces a significant contribution to the hard XRB.

6. Summary

With a 0.5–10 keV luminosity of 1.6×10^{42} ergs s^{-1}, NGC 3256 is the most X-ray–luminous starburst galaxy currently known. Our optical spectroscopy and deep, high-resolution soft X-ray image of this object indicate that, similar to other nearby galaxies undergoing intense nuclear bursts of star formation, NGC 3256 has a significant amount of ionized gas in its halo that appears to possess all the characteristics of a "superwind." We associate this gas with the 0.3 keV thermal component found in our model for the broadband *ASCA* spectrum of NGC 3256. A second thermal component in this spectrum, with $kT = 0.8$ keV, is likely to be associated with supernova-heated gas confined to the starburst region itself. Our calculations indicate that the star formation in NGC 3256 is fully capable of supplying the mass and energy contained in these hot plasmas.

Hard X-rays are detected from NGC 3256 with energies up to 10 keV. Contrary to expectations that such emission in starburst galaxies is produced mainly by high-mass X-ray binary systems, our comparison of the stellar population in NGC 3256 with nearby star-forming regions indicates that HMXBs are unable to account for more than $\sim 20\%$ of the galaxy's hard X-ray luminosity. Despite the detection of broad Hα features in the extended emission-line regions, we find no evidence for

a buried active nucleus in this object. We have shown that inverse-Compton scattered emission, involving infrared photons and relativistic electrons produced as a result of the vigorous star formation in NGC 3256, is likely to provide a substantial fraction of its high-energy flux. The assumption that inverse-Compton scattering is generally responsible for the majority of the hard X-ray emission of star-forming galaxies explains the coincidence in spectral slope between faint radio sources and the hard XRB. Independent of the nature of the X-ray emission from starbursts, however, we find that these objects can make a significant contribution to the hard X-ray background.

We begin by acknowledging the extraordinarily thorough and helpful report of the referee, Prof. T. Heckman; incorporation of his input has improved this paper significantly. We also thank the staff at CTIO for the generous allocation of telescope time and for their assistance obtaining the optical data presented in this paper. We are indebted to Rob Petre for his assistance with the planning of the *ASCA* observation, and to Amiel Sternberg for many helpful discussions about starburst galaxies. Our research has made use of *ROSAT* archival data obtained through the High Energy Astrophysics Science Archive Research Center (HEASARC) at NASA Goddard Space Flight Center. This work has been generously supported by NASA through grants NAG5-2556, NGG5-6035, and NAG5-3556. ECM acknowledges partial support by NASA through Chandra Fellowship grant PF8-10004 awarded by the Chandra X-ray Center, which is operated by the Smithsonian Astrophysical Observatory for NASA under contract NAS8-39073. The work of MDL was funded through the Dutch Organization for Research (NWO) and the Dutch Ministry of Education. Support for ECM and MDL at IGPP/LLNL was provided by the U.S. Department of Energy under contract W-7405-ENG-48. DJH thanks the Institute of Astronomy, University of Cambridge and the Raymond and Beverly Sackler Foundation for hospitality and support during the completion of this work. This is contribution number 667 of the Columbia Astrophysics Laboratory.

REFERENCES

Armus, L., Heckman, T. M., Weaver, K. A., & Lehnert, M. D. 1995, ApJ, 445, 666
Awaki, H., Ueno, S., Koyama, K., Tsuru, T., & Iwasawa, K. 1996, PASJ, 48, 409
Benn, C. R., Rowan-Robinson, M., McMahon, R. G., Broadhurst, T. J., & Lawrence, A. 1993, MNRAS, 263, 98
Boller, T., Meurs, E. J. A., Brinkmann, W., Fink, H., Zimmermann, U., & Adorf, H.-M. 1992, A&A, 261, 57
Bookbinder, J., Cowie, L. L., Krolik, J. H., Ostriker, J. P., & Rees, M. 1980, ApJ, 237, 647
Bradt, H. V. D., & McClintock, J. E. 1983, ARA&A, 21, 13
Comastri, A., Setti, G., Zamorani, G., & Hasinger, G. 1995, A&A, 296, 1
Condon, J. J. 1989, ApJ, 338, 13
Dahlem, M., Hartner, G. D., & Junkes, N. 1994, ApJ 432, 598
Dahlem, M., Heckman, T. M., Fabbiano, G., Lehnert, M. D., & Gilmore, D. 1996, ApJ, 461, 724
Dalton, W. W., & Sarazin, C. L. 1995, ApJ, 440, 280
David, L. P., Jones, C., & Forman, W. 1992, ApJ, 388, 82
Day, C., Arnaud, K., Ebisawa, K., Gotthelf, E., Ingham, J., Mukai, K., & White, N. 1995, The ABC Guide to *ASCA* Data Reduction (Greenbelt: NASA/GSFC)
Della Ceca, R., Griffiths, R. E., & Heckman, T. M. 1997, ApJ, 485, 581
Della Ceca, R., Griffiths, R. E., & Heckman, T. M., & MacKenty, J. W. 1996, ApJ, 469, 662
Edmunds, M. G., & Pagel, B. E. J. 1984, MNRAS, 211, 507
Fabbiano, G. 1988, ApJ, 330, 672
Fabbiano, G. 1989, ARA&A, 27, 87
Fabian, A. C., & Barcons, X. 1992, ARA&A, 30, 429
Feast, M. W., & Robertson, B. S. C. 1978, MNRAS, 185, 31

Fomalont, E. B., Windhorst, R. A., Kristian, J. A., & Kellermann, K. I. 1991, AJ, 102, 1258
Gendreau, K. C., et al. 1995, PASJ, 47, L5
Graham, J. R., Wright, G. S., Meikle, W. P. S., & Joseph, R. D. 1984, Nature, 310, 213
Griffiths, R. E., & Padovani, P. 1990, ApJ, 360, 483
Haarsma, D. B., & Partridge, R. B. 1998, ApJ, 503, L5
Hargrave, P. J. 1974, MNRAS, 168, 491
Hasinger, G., Burg, R., Giacconi, R., Schmidt, M., Trümper, J., & Zamorani, G. 1998, A&A, 329, 482
Heckman, T. M. 1980, A&A, 87, 152
Heckman, T. M. 1998, in Origins, eds. C. E. Woodward, J. M. Shull, & H. A. Thronson, ASP Conference Series, 148, 127
Heckman, T. M., Armus, L., & Miley, G. K. 1990, ApJS, 74, 833
Heckman, T. M., Dahlem, M., Eales, S. A., Fabbiano, G., & Weaver, K. 1996, ApJ, 457, 616
Heckman, T. M., Dahlem, M., Lehnert, M. D., Fabbiano, G., Gilmore, D., & Waller, W. H. 1995, ApJ, 448, 98
Helfand, D. J., & Moran, E. C. 1999, ApJ, in preparation
Helou, G., Khan, I. R., Malek, L., & Boehmer, L. 1988, ApJS, 68, 151
Helou, G., Soifer, B. T., & Rowan-Robinson, M. 1985, ApJ, 298, 7
Joseph, R. D., & Wright, G. S. 1985, MNRAS, 214, 87
Kotilainen, J. K., Moorwood, A. F. M., Ward, M. J., & Forbes, D. A. 1996, A&A, 305, 107
Kron, R. G., Koo, D. C., & Windhorst, R. A. 1985 A&A, 146, 38
Lehnert, M. D., & Heckman, T. M. 1994, ApJ, 426, L27
Lehnert, M. D., & Heckman, T. M. 1995, ApJS, 97, 89
Lehnert, M. D., & Heckman, T. M. 1996, ApJ, 462, 651
Leitherer, C., & Heckman, T. M. 1995, ApJS, 96, 9
Leitherer, C., Robert, C., & Drissen, L. 1992, ApJ, 401, 596
Lutz, D., et al. 1996, A&A, 315, L137
Madau, P., Ghisellini, G., & Fabian, A. C. 1994, MNRAS, 270, L17
Mather, J. C., et al. 1990, ApJ, 354, L37
McCarthy, P. J., Heckman, T., & van Breugel, W. 1987, AJ, 92, 264
Mihos, J. C., & Hernquist, L. 1996, ApJ, 464, 641
Miley, G. 1980, ARA&A, 18, 165
Moorwood, A. F. M., & Oliva, E. 1994, ApJ, 429, 602
Moran, E. C., Halpern, J. P., & Helfand, D. J. 1994, ApJ, 433, L65
Moran, E. C., & Lehnert, M. D. 1997, ApJ, 478, 172
Nagase, F. 1989, PASJ, 41, 1
Nandra, K., & Pounds, K. A. 1994, MNRAS, 268, 405
Norris, R. P., & Forbes, D. A. 1995, ApJ, 446, 594
Ohashi, T., & Tsuru, T. 1992, in Frontiers of X-ray Astronomy (Tokyo: Universal Academy Press), 435
Osterbrock, D. E. 1989, Astrophysics of Gaseous Nebulae and Active Galactic Nuclei (Mill Valley: University Science Books)
Portegies Zwart, S. F., & Verbunt, F. 1996, A&A 309, 179
Ptak, A., Serlemitsos, P., Yaqoob, T., Mushotzky, R., & Tsuru, T. 1997, AJ, 113, 1286
Rephaeli, Y., Gruber, D., Persic, M., & MacDonald, D. 1991, ApJ, 380, L59
Reynolds, R. J. 1990, in IAU Symp. 114, The Interstellar Disk-Halo Connection in Galaxies, ed. H. Bloeman (Dordrecht: Kluwer), 67
Richards, E. A., Kellermann, K. I., Fomalont, E. B., Windhorst, R. A., & Partridge, R. B. 1998, AJ, 116, 1039
Richards, E. A. 1998, BAAS, 30, 1326

Rieke, G. H., Lebofsky, M. J., Thompson, R. I., Low, F. J., & Tokunaga, A. T. 1980, ApJ, 238, 24
Rigopoulou, D., et al. 1996 A&A, 315, L125
Sanders, D. B., Soifer, B. T., Elias, J. H., Madore, B. F., Matthews, K., Neugebauer, G., & Scoville, N. Z. 1988, ApJ, 325, 74
Sargent, A. I., Sanders, D. B., & Phillips, T. G. 1989, ApJ, 346, L9
Sargent, W. L. W., & Filippenko, A. V. 1991, AJ, 102, 107
Schaaf, R., Pietsch, W., Biermann, P. L., Kronberg, P. P., & Schmutzler, T. 1989, ApJ, 336, 722
Schmidt, M., et al. 1998, A&A, 329, 495
Steidel, C. C., Adelberger, K. L., Giavalisco, M., Dickinson, M., & Pettini, M. 1999, ApJ, in press
Stewart, G. C., Fabian, A. C., Terlevich, R. J., & Hazard, C. 1982, MNRAS, 200, 61P
Strickland, D. K., Ponman, T. J., & Stevens, I. R. 1997, A&A, 320, 378
Suchkov, A. A., Balsara, D., Heckman, T. M., & Leitherer, C. 1994, ApJ, 430, 511
Suchkov, A. A., Berman, V. G., Heckman, T. M., & Balsara, D. S. 1996, ApJ, 463, 528
Sutherland, R. S., & Dopita, M. A. 1993, ApJS, 88, 253
Tanaka, Y., Inoue, H., & Holt, S. S. 1994, PASJ, 46, L37
Tenorio-Tagle, G., Muñoz-Tuñónm C., Pérez, E., & Melnick, J. 1997, ApJ, 490, L179
Thuan, T. X., & Condon, J. J. 1987, ApJ, 322, L9
Tucker, W. H. 1975, Radiation Processes in Astrophysics (Cambridge: MIT Press), 169
Vacca, W. D. 1994, ApJ, 421, 140
van Paradijs, J. 1995 in X-ray Binaries, eds. W. H. G. Lewin, J. van Paradijs, & E. P. J. van den Heuvel (Cambridge: Cambridge University Press), 536
Veilleux, S., & Osterbrock, D. E. 1987, ApJS, 63, 295
Voges, W., et al. 1996, IAU Circ. 6420
Wang, J., Heckman, T., & Lehnert, M. D. 1997, ApJ, 491, 114
Weedman, D. W. 1987, in Star Formation in Galaxies, ed. C. J. Lonsdale (NASA CP-2466), 351
White, N., Swank, J., & Holt, S. 1983, ApJ, 270, 711
Windhorst, R. A., et al. 1995, Nature, 375, 471
Windhorst, R. A., Fomalont, E. B., Partridge, R. B., & Lowenthal, J. D. 1993, ApJ, 405, 498
Windhorst, R. A., Miley, G. K., Owen, F. N., Kron, R. G., & Koo, D. C. 1985, ApJ, 289, 494
Wright, E. L., et al. 1994, ApJ, 420, 450
Yaqoob, T., Serlemitsos, P. J., Ptak, A., Mushotzky, R., Kunieda, H., & Terashima, Y. 1995, ApJ, 455, 508

TABLE 1

FITS TO THE *ASCA* SPECTRA OF NGC 3256

Components In Model	Component[a]	kT (keV) or Γ	$N_{\rm H}$ ($\times 10^{21}$ cm^{-2})	A[b]	Model χ^2 (ν)
1	R-S	0.78	8.4	18.7	206.8 (82)
2	R-S	4.14	6.5	5.0	96.7 (80)
	R-S	0.73	[c]	10.4	
2	R-S	11.80	0.0	3.6	83.7 (79)
	R-S	0.68	7.9	12.8	
2	PL	2.40	3.3	3.3	92.4 (80)
	R-S	0.81	[c]	3.6	
2	PL	$1.67^{+0.72}_{-0.45}$	$0.0^{+3.3}_{-0.0}$	1.2	80.7 (79)
	R-S	$0.75^{+0.10}_{-0.16}$	$7.2^{+2.1}_{-3.4}$	9.9	
3	PL	$1.68^{+0.84}_{-1.22}$	$7.9^{+1.9}_{-3.2}$	1.2	69.8 (78)
	R-S	$0.80^{+0.16}_{-0.15}$	[c]	13.0	
	R-S	$0.29^{+0.40}_{-0.14}$	1.0[d]	1.1	

[a] PL = power law; R-S = Raymond-Smith plasma; TB = thermal bremsstrahlung.

[b] Component normalization at 1 keV. For PL components, A has units of 10^{-4} photons cm^{-2} s^{-1} keV^{-1}; for R-S components, A is equal to $[10^{-18}/4\pi D^2] \int n_e^2 dV$, where D is the distance to the source in cm, n_e is the electron density in cm^{-3}, and V is the volume of the emitting region in cm^3.

[c] Absorption column density same as that applied to first component in this model.

[d] Absorption column density fixed at the Galactic value.

NOTES.—Indicated errors are 90% confidence limits for four interesting parameters ($\Delta\chi^2 = 7.78$). Solar abundances are assumed for all R-S components.

TABLE 2

FLUXES AND LUMINOSITIES FOR THE THREE-COMPONENT MODEL

	0.1–2.4 keV		0.5–2.0 keV		2.0–10.0 keV		0.1–10.0 keV	
Component	F_X[a]	L_X[b]	F_X[a]	L_X[b]	F_X[a]	L_X[b]	F_X[a]	L_X[b]
PL	1.05	1.87	0.71	0.99	4.58	1.86	5.30	3.56
R-S (warm)	5.23	16.3	4.78	12.2	1.28	0.62	6.05	16.7
R-S (soft)	1.53	1.27	1.41	0.86	0.00	0.00	1.53	1.27
Total	7.81	19.4	6.90	14.0	5.86	2.48	12.9	21.5

[a] Observed X-ray flux in units of 10^{-13} ergs cm^{-2} s^{-1}.

[b] Intrinsic (unabsorbed) X-ray luminosity in units of 10^{41} ergs s^{-1}.

Figure Captions

Fig. 1.—Optical emission-line flux ratios as a function of offset from the nucleus of NGC 3256 along PA = 65°, before (*filled squares*) and after (*open squares*) correction for extinction and Balmer absorption in the underlying stellar continuum. Positive offsets are west-southwest of the nucleus.

Fig. 2.—Emission-line flux ratios as a function of offset from the nucleus of NGC 3256 along PA = 155°, before (*filled squares*) and after (*open squares*) correction for extinction and Balmer absorption in the underlying stellar continuum. Positive offsets are north-northwest of the nucleus.

Fig. 3.—Spectra of the nuclear (*upper panel*) and off-nuclear (*middle and lower panels*) regions of NGC 3256 along PA = 155°. The line-flux ratios in the nuclear spectrum are typical of H II regions. The off-nuclear spectra, representing 8″ extractions centered 18″ (4.9 kpc) from the nucleus, exhibit enhancements of the low-ionization [O I] λ6300, [N II] $\lambda\lambda$6548, 6583, and [S II] $\lambda\lambda$6716, 6731 emission lines, similar to the ionized gas observed in the halos of edge-on starburst galaxies. The weak, broad Hα line present in the off-nuclear spectra is observed in *all* extended emission-line regions sufficiently distant from the nucleus.

Fig. 4.—Emission-line velocity widths as a function of offset from the nucleus of NGC 3256 along PA = 155°. The width of Hα does not include the contribution from a broad component (see Fig. 3), if present.

Fig. 5.—The [O I]/Hα flux ratio (corrected for both reddening and Balmer absorption) vs. Hα velocity width in NGC 3256. The apparent correlation supports the notion that the off-nuclear emission in the galaxy is the result of a shock-ionized wind. The width of Hα does not include the contribution from a broad component (see Fig. 3), if present.

Fig. 6.—Contours from the *ROSAT* HRI image of NGC 3256, overlayed on an optical image from the Digitized Sky Survey. To emphasize the low surface brightness X-ray emission, we binned the HRI image to have 4″ pixels and then smoothed it with a $\sigma_G = 6''$ Gaussian. The contours correspond to values of 1, 2.5, 4, 7, 11, and 15 (smoothed) counts per pixel. The axes are labeled with J2000 coordinates. The soft X-ray emission is confined to the main body of the galaxy, but extends over a 12 kpc diameter.

Fig. 7.—The 0.5–10 keV *ASCA* spectrum of NGC 3256. (*a*) The observed spectrum and best-fitting two-component (PL + R-S) model (folded through the instrument response functions) are plotted in the upper panel. The unfolded spectrum shown in the lower panel indicates that, in this model, the power-law component must dominate at both hard and very soft X-ray energies. In (*b*), the three-component model from Table 1 has been applied. The upper panel shows that this model provides a slightly better fit than the two-component model. As the unfolded spectrum displayed in the lower panel indicates, the power-law, warm (0.8 keV) thermal, and soft thermal components dominate in the hard, medium-energy ($\sim$ 0.8–2 keV), and very soft bands, respectively.

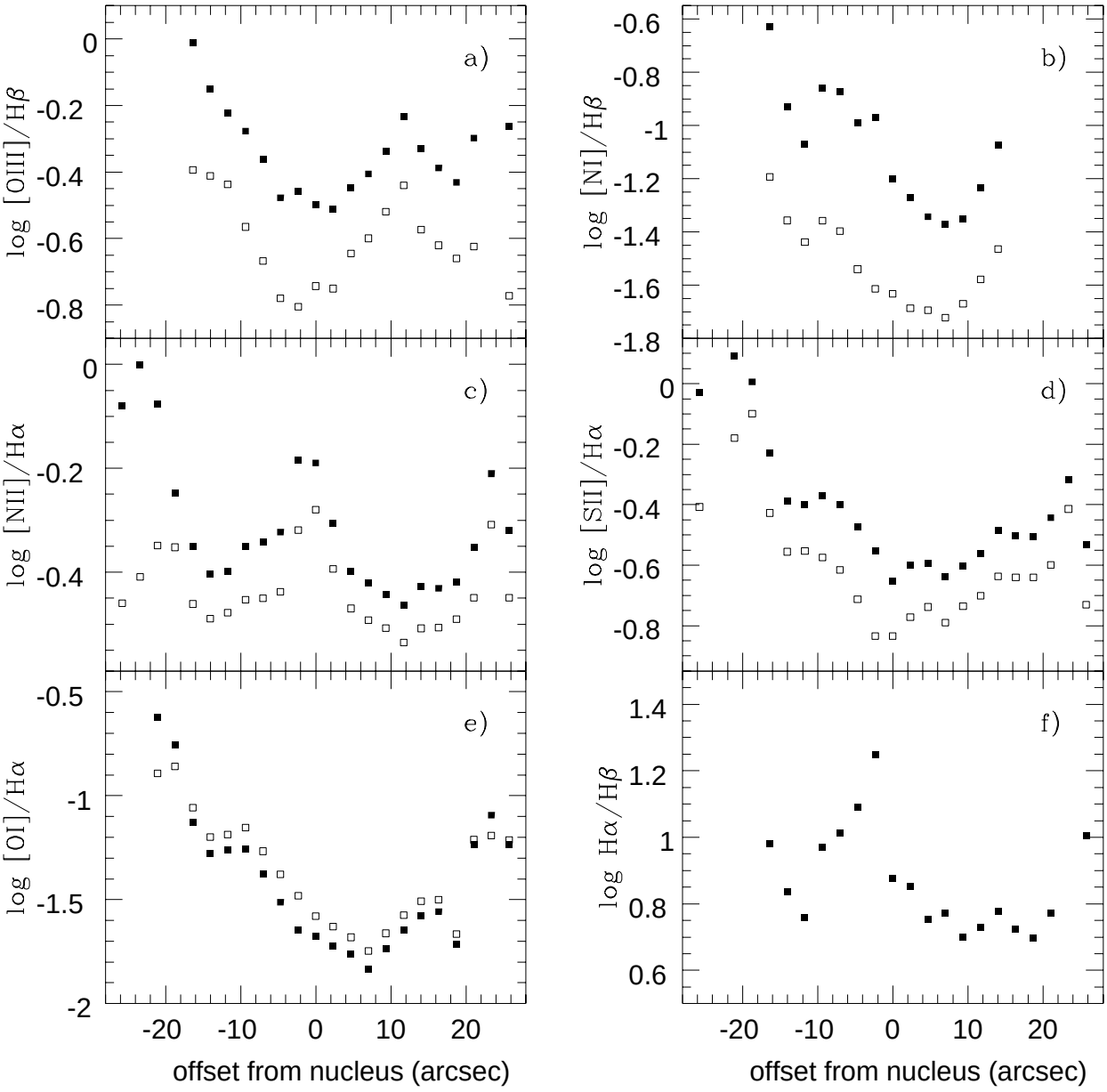
a)
b)
c)
d)
e)
f)
log [OIII]/Hβ
log [NI]/Hβ
log [NII]/Hα
log [SII]/Hα
log [OI]/Hα
log Hα/Hβ
offset from nucleus (arcsec)
offset from nucleus (arcsec)

FIG. 1

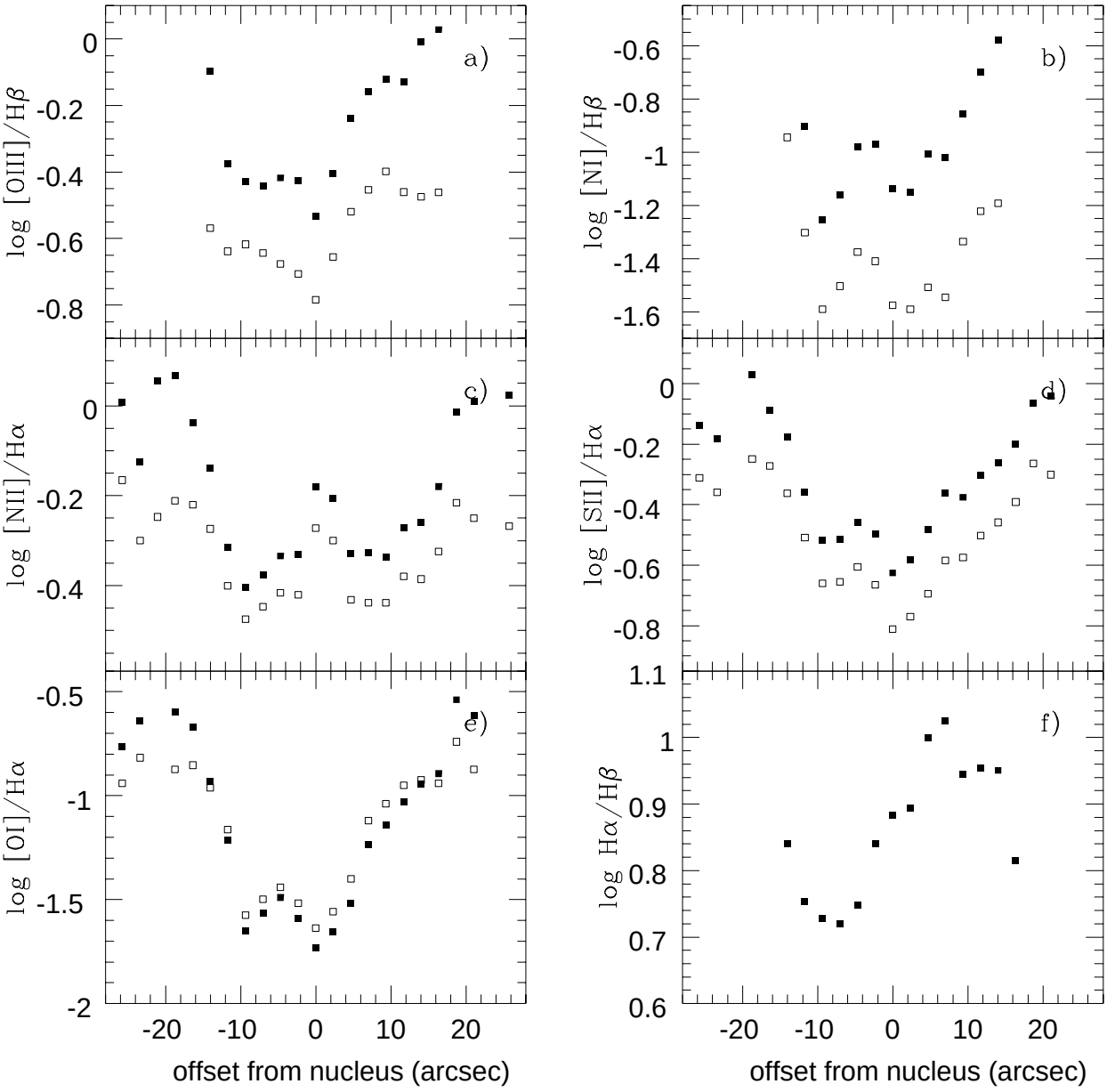
a)
b)
c)
d)
e)
f)
log [OIII]/Hβ
log [NI]/Hβ
log [NII]/Hα
log [SII]/Hα
log [OI]/Hα
log Hα/Hβ
offset from nucleus (arcsec)
offset from nucleus (arcsec)

FIG. 2

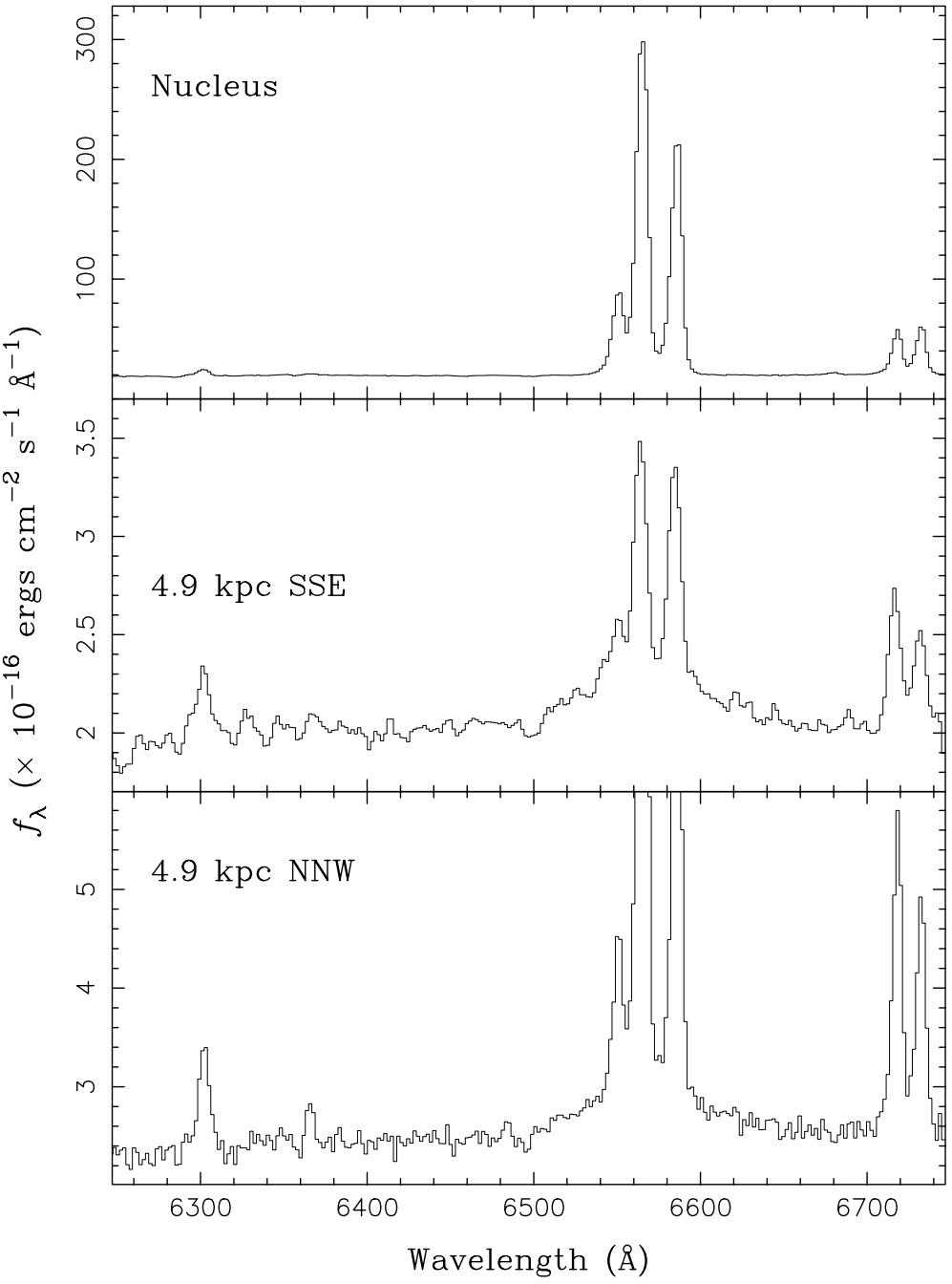
Nucleus
4.9 kpc SSE
4.9 kpc NNW
f_λ ($\times 10^{-16}$ ergs cm^{-2} s^{-1} Å^{-1})
Wavelength (Å)
6300
6400
6500
6600
6700
100
200
300
2
2.5
3
3.5
3
4
5

FIG. 3

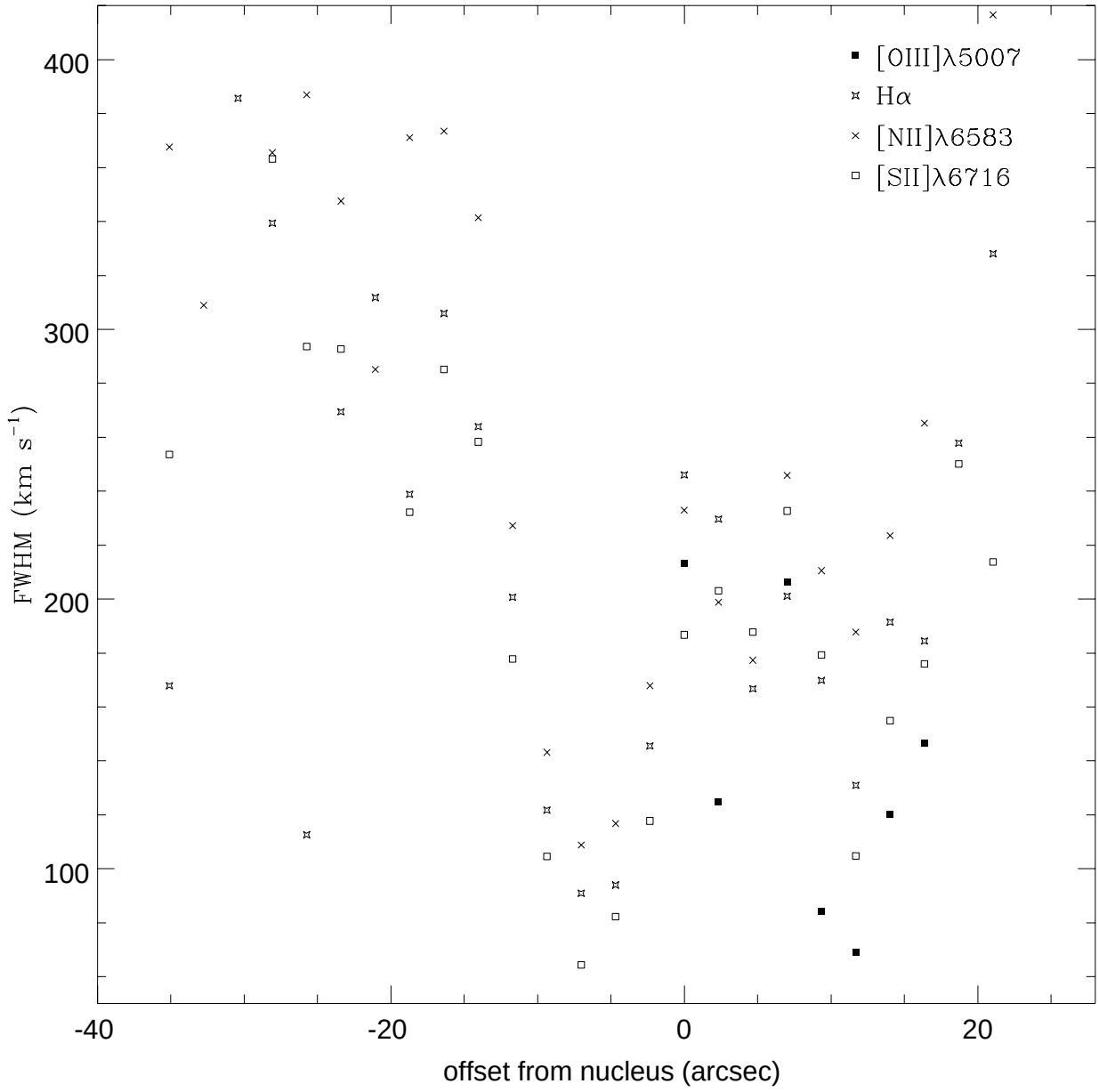
[OIII]λ5007
Hα
[NII]λ6583
[SII]λ6716
FWHM (km s^{-1})
400
300
200
100
-40
-20
0
20
offset from nucleus (arcsec)

FIG. 4

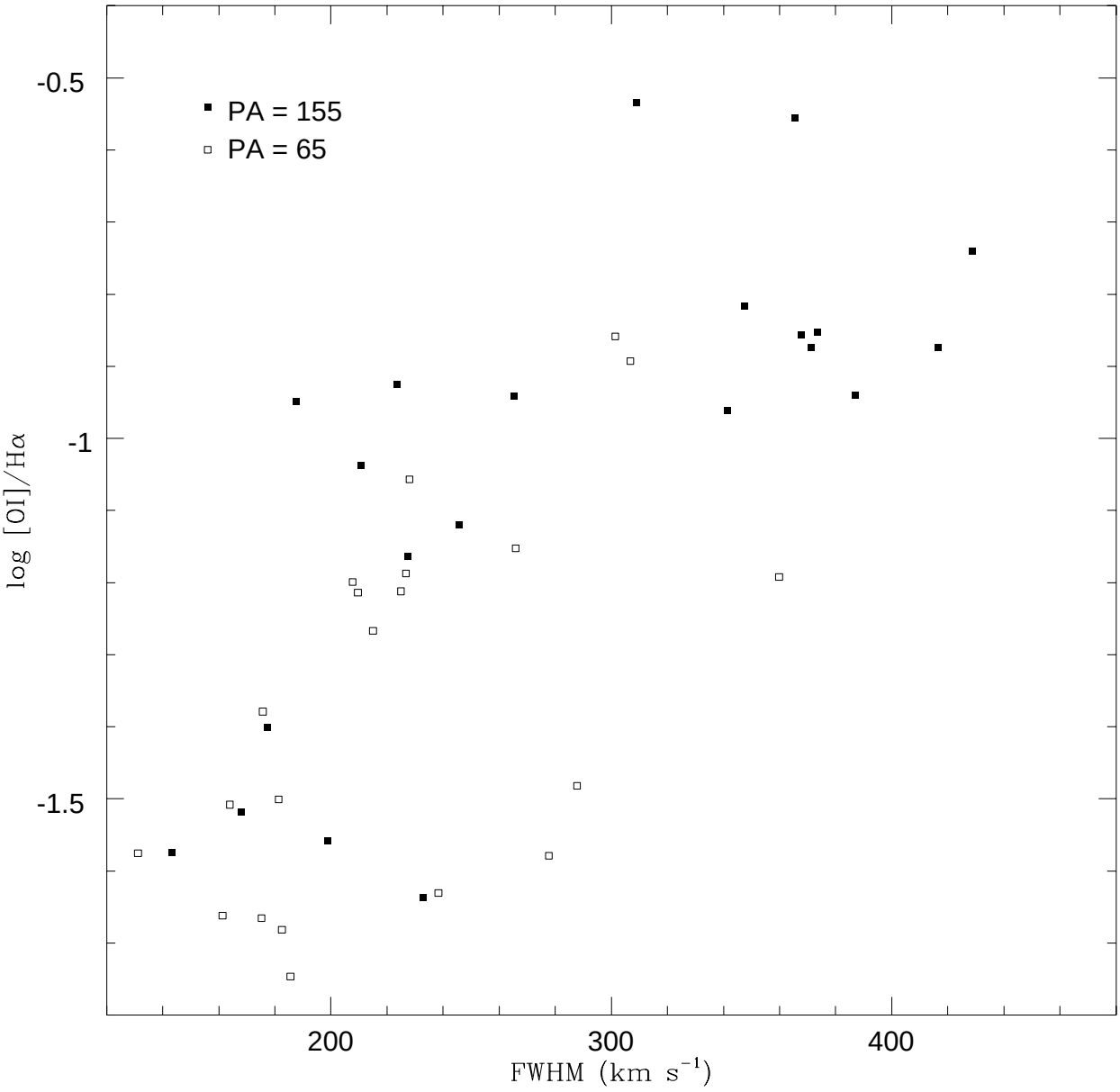

FIG. 5

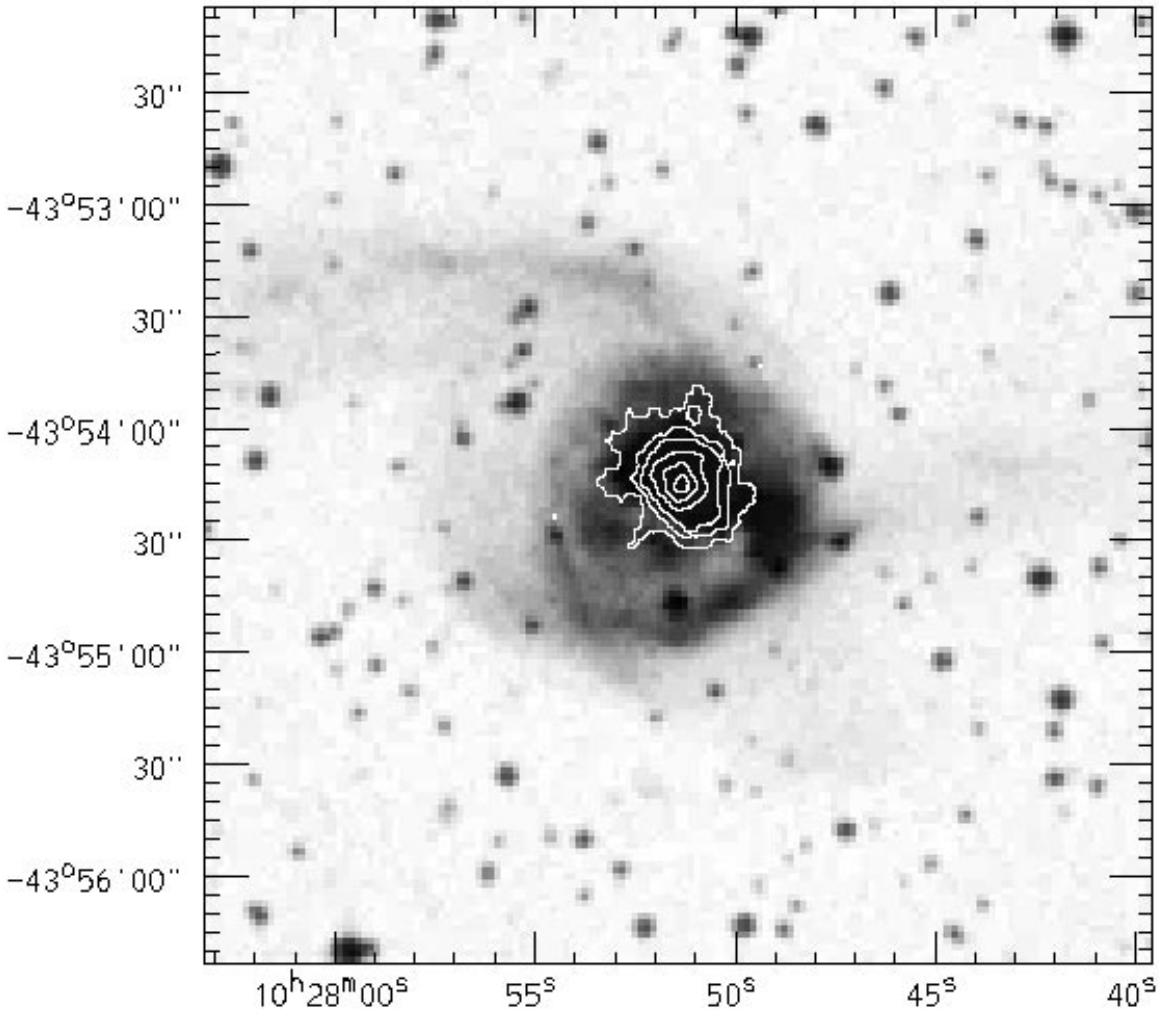
30''
-43°53'00"
30''
-43°54'00"
30''
-43°55'00"
30''
-43°56'00"
10h28m00s
55s
50s
45s
40s

FIG. 6

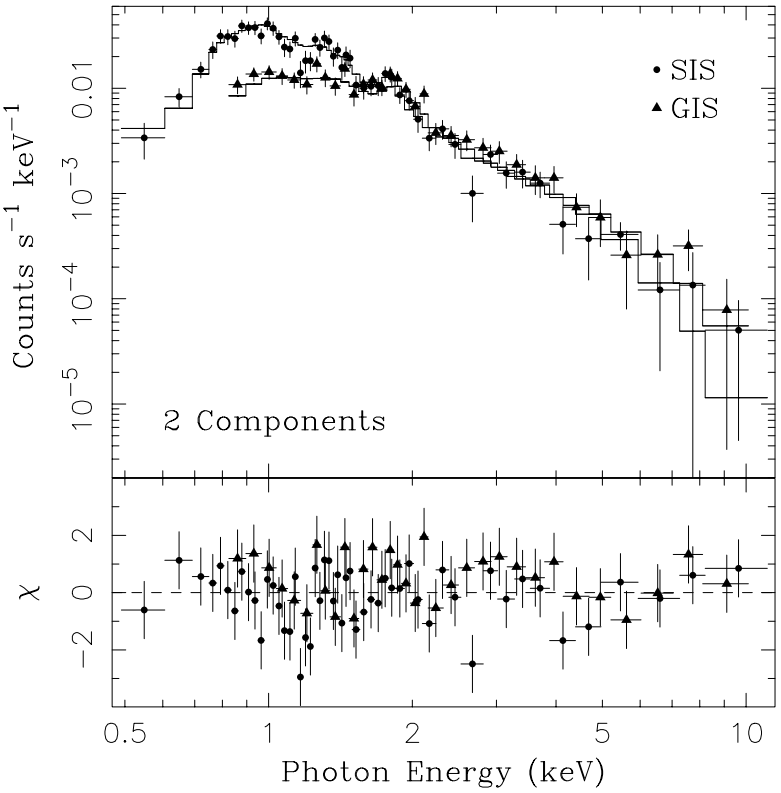
Counts s^{-1} keV^{-1}
SIS
GIS
2 Components
χ
Photon Energy (keV)

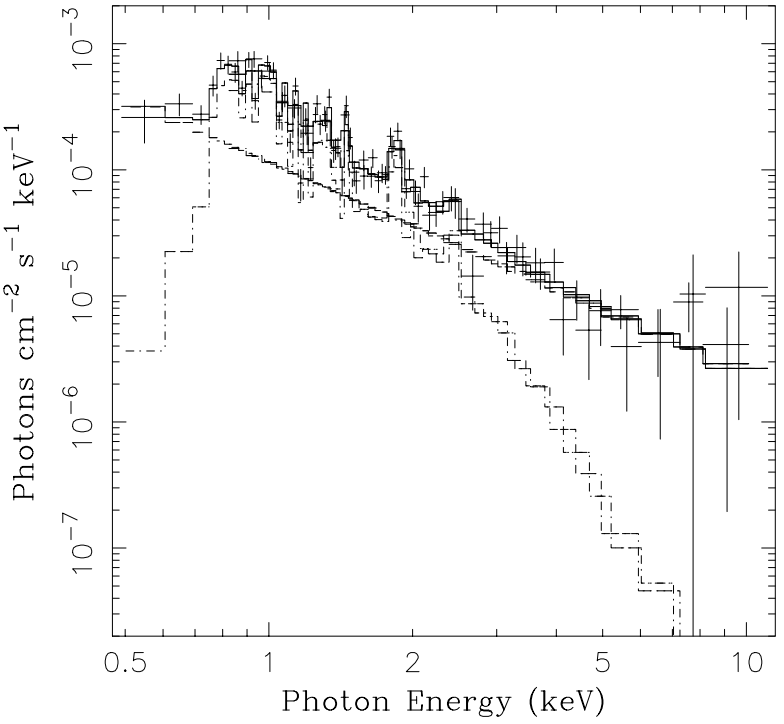
Photons cm^{-2} s^{-1} keV^{-1}
Photon Energy (keV)

FIG. 7*a*

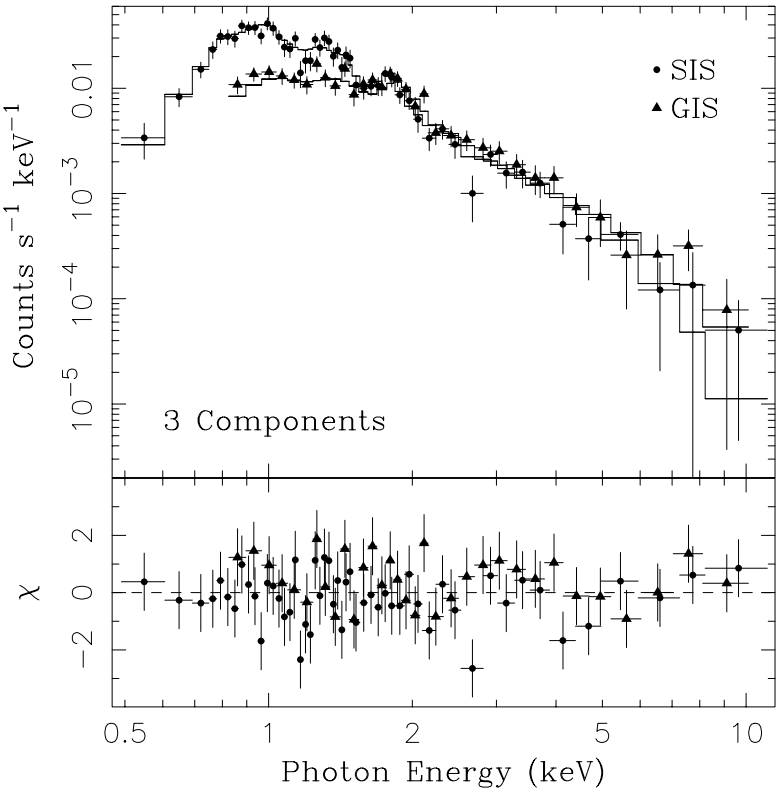
Counts s^{-1} keV^{-1}
0.01
10^{-3}
10^{-4}
10^{-5}
• SIS
▲ GIS
3 Components
χ
2
0
−2
0.5
1
2
5
10
Photon Energy (keV)

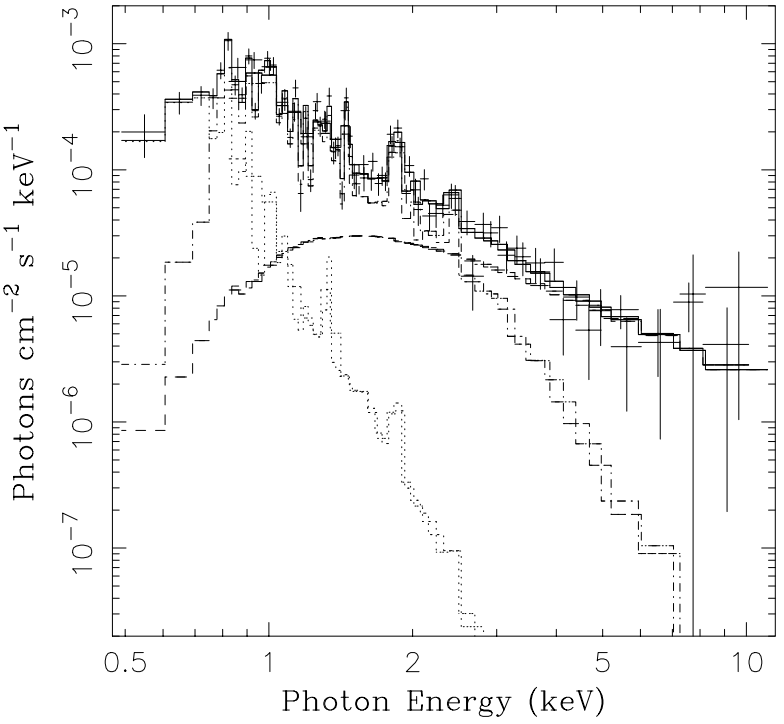
Photons cm^{-2} s^{-1} keV^{-1}
10^{-3}
10^{-4}
10^{-5}
10^{-6}
10^{-7}
0.5
1
2
5
10
Photon Energy (keV)

FIG. 7*b*